

# Horizontally Integrated Remote Measurements of Ocean Currents Using Acoustic Tomography Techniques

## Chapter Outline

7.1. One-Way Tomography	203	7.6. Acoustic Tomographic Measurements of Vorticity	230
7.2. Two-Way Tomography (Reciprocal Tomography)	210	7.7. Horizontally Integrated Current Measurements Using Space-Time Acoustic Scintillation Analysis Technique	232
7.3. Acoustic Tomographic Measurements from Straits	212		
7.4. Coastal Acoustic Tomography	215	References	235
7.5. River Acoustic Tomography	226	Bibliography	237

Satellite remote-sensing techniques, employing active and passive optical, thermal, and microwave signals, and coastally operated remote-sensing techniques employing active electromagnetic signals in the HF, VHF, UHF and microwave bands are used on an operational scale for remote detection and quantitative mapping of ocean surface current vectors and circulation patterns. However, the inability of electromagnetic signals to penetrate below the surface layer of the ocean has rendered these techniques unusable for remote measurements of subsurface currents and their circulation features. Physical oceanographers have an interest in subsurface current measurements to gain insight into the water circulation in the ocean layers at various depths and its dependence and possible effects on climatological conditions. Apart from this, subsurface currents are of considerable importance in marine geology because of their influence on the transportation and deposition of sediment. Knowledge of deep currents is also of interest to biologists because of the currents' influence on the dispersal of organisms and the maintenance of supplies of nutrients. Regions of convergence or divergence in the horizontal movements of water mass are of particular interest because of their association with vertical movements in the form of sinking or upwelling.

The traditional means of making observations of subsurface currents was an indirect one, the so-called *dynamical method*, based on highly precise measurements

of water temperature, salinity, and depth; the hydrographic tables for computing density; the geostrophic equation; and an assumption regarding the “depth of no motion.” The valuable review of Bowden (1954) focuses attention on the assumptions made and uncertainties involved in the dynamical computations regarding the depth of no motion and the mean subsurface current charts. In fact, Stommel's (1955) letter to the editor provides an indication of an almost total lack of knowledge on subsurface currents in the early 1950s.

For lack of proper tools, direct measurements of subsurface currents were limited to those made from current meters tethered from anchored ships, moored current meters, freely sinking/rising vertical profilers, and so on. An example whereby much effort has been expended with a large variety of techniques is the Straits of Florida. Current meter moorings (Lee et al., 1985), Pegasus sections (Leaman et al., 1995), sea-level differences (Maul et al., 1985), and undersea cables (Larsen and Sanford, 1985) have all been employed for measuring the water-current flow there. For a variety of reasons, such limited measurements were not adequate to resolve the spatial structure of deep-water motions. Tracking of subsurface drifters (see Chapter 6) yielded Lagrangian descriptions of subsurface currents. However, these tools were inadequate to provide basin-scale horizontally integrated current measurements.

Since the infancy of oceanographic research, oceanographers have been strapped for observations over large regions of the ocean in anything like rapid enough time to get synoptic views or snapshots. If one goes out and surveys a large region of the ocean with a ship, the ocean might have already changed by the time the survey is completed.

The situation faced by oceanographic researchers is quite different from the situation of meteorologists, who can get virtually instantaneous pictures of the atmosphere from either a global measuring network or satellite images of clouds and so forth. They really do get images that are, effectively, snapshots. In contrast, oceanographers are not so fortunate, with the exception of satellite maps of surface temperature, color, and roughness and possibly, satellite altimetry measurements used as sea surface tomography. But none of these measurements extends beneath the surface. It was hoped that acoustic transmissions and receptions could well turn out to be one of the few ways to acquire measurements of what is happening in the ocean over a large spatial scale fast enough that one is not hopelessly mixed up between time variations and space variations.

*Ocean acoustic tomography* (OAT) is a method employed in measuring the ocean by utilizing the favorable properties of sound propagation through water. The outlines of such a system (i.e., the feasibility of monitoring and ultimately studying the oceans by measuring acoustic transmissions between moorings over large distances) were originally proposed by Walter Munk (Scripps Institution of Oceanography) and Carl Wunsch (Massachusetts Institute of Technology), as provided in [Munk and Wunsch \(1979\)](#). In subsequent years there has been a substantial effort to demonstrate both the practicality of the idea ([Spiesberger et al., 1980](#)) and to further analyze the theoretical aspects of sound propagation in this context ([Munk and Wunsch, 1982a,b, 1983; Spofford and Stokes, 1984](#)). The theory was further developed and tested to a large part with active contribution from Robert Spindel (Woods Hole Oceanographic Institution).

Ocean acoustic tomography techniques have been developed for remote measurements of large-scale subsurface currents and the associated large-scale circulation features. Similar to the use of X-rays to produce medical computer-assisted tomography (CAT) scans in hospitals to examine the interior of the human body and the use of seismic waves by geophysicists to determine the Earth's internal structure, OAT employs low-frequency sound waves to probe large sections of the oceans. Ocean tomography describes, layer by layer, the interior features of the ocean by transmitting sound waves along many transmitter-to-receiver paths between distantly spaced instrument moorings. The details of the ocean's interior are revealed by interpreting the arrival times of the sounds, since their speed is either accelerated or decelerated by the

temperature and current of the interior ocean. By transmitting sound waves through hundreds of miles of ocean, it becomes possible to make measurements over an area that would otherwise require a fleet of ships working for many weeks. With OAT it becomes possible to take a look at large-scale ocean circulation in a synchronous manner, which is a requirement to better understand a fundamental problem in oceanography. No other technique has the potential to make these ocean-interior measurements. The appeal of acoustical techniques is several-fold ([Cornuelle et al., 1985](#)):

1. Tomography techniques are by nature *integrating*, automatically filtering out undesirable small-scale features that "contaminate" normal point measurements. The unwanted features can range from microstructure and internal waves, if one's interest is in the mesoscale (order 100 kilometers), to the mesoscale itself, if one's interest is in the gyre-scale circulation.
2. In principle, the information content of tomographic arrays grows quadratically with the number  $N$  of moorings deployed rather than approximately linearly, as with conventional point moorings. It may be noted that over long distances, a source may not be heard by all receivers, and the addition of new instruments thus may not provide information quite as fast as  $N^2$ .
3. As a consequence of the waveguide nature of sound propagation over much of the ocean, a single source-receiver pair can provide information about the horizontal average of the vertical structure of oceanic disturbances that would otherwise require large numbers of vertically distributed instruments.

The theory on paper advanced to sea in two tests conducted in the Atlantic Ocean during 1981 and 1983 and subsequent tests funded by the U.S. National Science Foundation (NSF) and the Office of Naval Research (ONR). Each at-sea test became more complicated as the tomography itself grew more sophisticated. There are essentially two kinds of tomography: (1) one-way tomography (called the *zero-order* kind of tomography) and (2) two-way tomography (called *reciprocal tomography*). The former is essentially measuring the temperature of the ocean by measuring the time it takes for sound to traverse from a source to a receiver; the latter measures the difference in time it takes to send a signal from a source to a receiver and back again.

Although the principle of OAT was well founded, its practical realization on an operational scale took a long time because the issues had to do more with engineering developments. The principles had been demonstrated, but it was necessary to develop better, cheaper, very reliable, long-lived sources and receivers. The science that could be developed with the application of acoustic tomography did not advance rapidly enough, because oceanographers had

to wait for the more complicated engineering to catch up to the need. The elaborate electronic equipment for the acoustic tomography experiment was not yet commercially available and had to be designed and built by the technologists at various oceanographic research institutions.

## 7.1. ONE-WAY TOMOGRAPHY

In one-way tomography, the travel time between moorings of the multipaths created by an acoustic pulse is very accurately measured, and the way the multipath travel times change over daily, weekly, and seasonal time periods is monitored. The fundamental simplicity of the idea of acoustic tomography is impressive. Sound propagation in the ocean is described by the equations of classical physics. In acoustic tomography, acoustic ray theory is used to compute sound propagation in a complex environment. It is unique in identifying which part of the ocean (in the intervening space between a source-receiver pair) is sampled by the sound signal corresponding to the arrival of each pulse. With the aid of computers it is economical to simulate measurements prior to the conduct of any field experiment. Ray theory is adopted for computing the trajectory of an acoustic signal based on the assumption that (1) the acoustic wavelength is much smaller than the local water depth, and (2) the change of sound speed is negligible over several wavelengths. Following Arthur et al. (1952), the ray geometry (Figure 7.1) is governed by the following equations:

$$\frac{dx}{ds} = \cos\theta \quad (7.1a)$$

$$\frac{dy}{ds} = \sin\theta \quad (7.1b)$$

$$\frac{d\theta}{ds} = \frac{1}{c} \left[ \frac{\partial c}{\partial x} \sin\theta - \frac{\partial c}{\partial y} \cos\theta \right] \quad (7.1c)$$

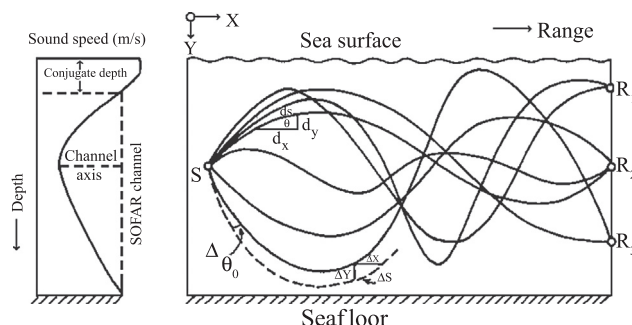


**FIGURE 7.1** Schematic presentation of the acoustic ray coordinate system. (Source: Kumar et al., 1994.)

In these expressions,  $\theta$  is the angle of emergence of the sound ray,  $s$  is the arc length along the ray, and  $c$  is the sound speed.  $ds$  represents an infinitesimal arc length along the ray, and  $dx$  and  $dy$  represent the corresponding infinitesimal lengths along the  $x$ -axis (i.e., the acoustic ray axis) and the  $y$ -axis, respectively. Numerical integration of these equations using available means (e.g., the Runge-Kutta technique) yields the eigen rays. Acoustic rays for various emergence angles are traced using appropriate software packages.

Tomography is based on the notion that if we can understand how sound propagates under specific physical conditions, we ought to be able to understand various aspects of the ocean through which the sound has passed. The concept of time-of-flight acoustic tomography to measure the ocean mesoscale was formulated in the late 1970s. The first demonstration of multipath resolution, stability, and identification through a 900-km propagation test was carried out in 1978. It was found that the individual arriving acoustic rays are identifiable, and that the rays are stable through time. Since then there has been an evolving (and expanding) research program involving at least a half a dozen institutions and many more scientists and engineers to test and evaluate the utility of the idea and to develop practical implementations. The mathematics of “inverse theory” (in many forms) provides us with convenient machinery for understanding the relationship between the measurements and the questions we have about how the ocean behaves (including the uncertainties with which quantities of interest are inferred). Based on these ideas, the measured multipath travel-time data are “inverted” by computer codes to obtain the temperature and current fields of the ocean, between the moorings of acoustic source-receiver pairs. Although the preliminary experiments supported the concept of tomography as a scientific tool, some researchers (e.g., Cornuelle et al., 1985) believed that a three-dimensional test of the method was necessary. It was felt that experience was needed with the second part of tomography—i.e., the “inversion.” As outlined by Munk and Wunsch (1979), one needs to take the “data” (i.e., the travel times of individual rays passing through a volume of ocean) and invert it to obtain information about the state of the ocean.

One-way tomography is employed in oceanography mainly to remotely detect mesoscale circulation features such as cold/warm-core eddy structures (known as the *ocean weather*) that are superimposed on a generally sluggish large-scale circulation (known as the *ocean climate*). The ocean mesoscale eddy field is closely analogous in character to weather systems in the atmosphere, but the two differ in terms of sizes and lifetimes. Whereas the oceanic eddy structures are several hundred kilometers in diameter and have lifetimes of a few months, the weather systems in the atmosphere are several thousand kilometers

in diameter and have lifetimes of a few days. Detection of mesoscale eddy structures in an ocean basin using acoustic one-way tomography relies on the measurement of travel time fluctuations induced by changes in the acoustic field within the ocean by acoustic transmission along many diverse paths. The first test, held in 1981 in areas north and west of Bermuda, involved the making of a three-dimensional, time-evolving map of the area.

In acoustic one-way tomography, sound sources are placed over a specified distance and give off signals. The signals, in turn, are picked up by receivers—essentially omnidirectional hydrophones—which are hung on moorings to record when a signal is received. The received signals can be used to determine water temperature, density, and current. With higher frequencies, bandwidth increases, which, in turn, makes timing of signals more accurate. However, high frequencies tend to be absorbed by the water medium because absorption increases with frequency. This, in turn, diminishes monitoring range. Therefore lower frequencies produce greater range but with less accuracy.

The sound speed in the ocean is predominantly a function of temperature and, to a lesser extent, salinity and water depth (Chen and Millero, 1977). Thus, a cold eddy within the observation region will delay the arrival of any transmission through the eddy, and a warm eddy will cause faster arrival of the acoustic transmission at the receiver. For example, in the Bay of Bengal in the Indian Ocean, an observed cold-core eddy of 5° temperature drop that brings about a reduction in the ambient sound speed by 10 m/s delays the travel times by 100 to 200 ms for a mesoscale range (Kumar et al., 1977).

As indicated earlier, the OAT technique involves two aspects, namely (1) the “forward” problem of finding the behavior of sound transmission in an ocean basin over distances of order 100 km, and (2) the “inverse” problem of determining the interior structure of this ocean basin from travel-time measurements of sound waves transmitted through the basin. In the OAT technique, the variable acoustic travel times between all source-receiver pairs of an array of underwater acoustic sources and receivers, moored at spatial intervals of usually more than 100 km, are used to construct the three-dimensional (time-variable) eddy field using inverse theory.

Munk and Wunsch (1979) simulated the inversion of real data by a method chosen primarily for its simplicity. Munk and Wunsch (1983) presented a finite amplitude (i.e., nonlinear) procedure for inverting tomographic data based on Abel transforms. Many superior inversion methods are available, all of which are intimately related (Herman, 1979, 1980). Inversion theories applied in various disciplines of science such as medical tomography, geophysics, and the like may be found in the literature (e.g., Liebelt, 1967; Bretherton et al., 1976; Parker, 1977; Aki and

Richards, 1980; Wunsch and Minster, 1982; Cornuelle, 1983; Zlotnicki, 1983), and the possible tradeoffs could only be studied with real data. An experiment conducted by Cornuelle et al. (1985) was the first attempt to use tomography as a full system at sea; it was in large measure an engineering demonstration. They wanted to try this novel system in a region of the ocean that was well understood and where there would be few, if any, surprises that could hamper an evaluation of the procedures. The at-sea experiment was thus deliberately conducted in an area that was congenial to focusing on the technology. Because of the rapid spatial coverage possible with tomography (the entire area was mapped once every three days), the experimenters did gain some valuable insight into the rapid time-evolution possible in mesoscale eddies.

To convert travel-time measurements to sound speed anomaly maps, they used the method often called the *stochastic inverse* in geophysics (Aki and Richards, 1980). Objective mapping in oceanography is a special case of this technique. The method assumes that an *a priori* estimate of the mean and covariance of the unknown field exists, and constructs an estimator which minimizes the square of the difference between the estimate of the unknown field and the true field at each point being mapped. A detailed discussion of this technique is given in Cornuelle et al. (1985).

The main element in any acoustic tomographic experiment is the acoustic transceiver, which functions both as an acoustic source and an acoustic receiver for hearing sounds from other transceivers. Early tomography transmitters were extensions of the technology employed by neutrally buoyant SOFAR floats, namely high-Q, open-end, resonant tubes, approximately one-quarter-wavelength long and driven at one end by a piezoelectric transducer. These devices had sound pressure levels approaching 180 dB re 1 µPa and bandwidths from 16 Hz at a center frequency of about 200 Hz (in 1980) to 100 Hz at a center frequency of about 400 Hz (in 1983). Signal-processing gains of some 35 dB yielded sound-pressure levels equivalent to 215 dB re 1 µPa. However, time resolution with 16-Hz bandwidth is barely adequate, and 100-Hz bandwidths are achievable only at higher frequencies where propagation loss is greater, thus restricting achievable ranges (Spindel and Worcester, 1991). For long-range experiments, hydraulic-acoustic sources, manufactured by Hydroacoustics Inc. (Rochester, New York), with 100-Hz bandwidth centered at 250 Hz, were used. Those sources had sound-pressure levels of 193 dB re 1 µPa, which, together with signal-processing gains, produced an equivalent 228-dB signal. Receivers (which were combined with these transmitters, thus producing transceivers) were equipped with four to six hydrophone vertical arrays to allow multipath discrimination by arrival angle as well as arrival time.

In another design, the sound was produced mechanically by a hydraulic piston that slightly bends an aluminum

sheet back and forth, making a 250-Hertz sound equivalent to a low hum. A powerful central microcomputer served as the supervisor of 18 single-chip microprocessors that performed individual tasks. Lithium batteries powered the system. To withstand the tremendous deep-sea pressures, the instruments were housed in inch-thick aluminum cylinders. More technologically advanced instruments were developed in subsequent years.

The great advantage of the OAT technique over conventional point measurements or ship surveys is that the number of data points grows geometrically as the product of the number of sources ( $S$ ), the number of receivers ( $R$ ), and the number of resolved acoustic paths ( $P$ ), compared with the sum ( $R + S$ ) for conventional spot measurements. This concept is demonstrated in Figure 7.2. Additionally, path integration reduces the noise from local fine structure and internal waves that contaminate spot measurements. The superb ability of the OAT technique is achieved essentially because of the transparency of ocean-to-acoustic signals and the presence of an acoustic waveguide known as the *SOFAR channel*. In the ocean there is a minimum sound-speed axis around 1-km depth. The sound speed above this axis gradually increases upward

because of increase in temperature, and it increases downward due to the effect of increasing pressure. This gradually increasing sound speed with reference to the acoustic axis corresponds to a gradually decreasing refractive index of the sound channel, because of which the acoustic ray within this channel travels long distances with minimal loss, in a manner similar to the propagation of light rays along an optical waveguide (Figure 7.3). Because the acoustic ray paths oscillate about the axis of the sound channel (i.e., the axis of minimum sound speed) these rays, depending on their inclination, can scan long distances in the vertical plane. It is interesting to note that the steep rays that traverse a large distance of the ocean in the vertical plane arrive at the receiver faster than those flat rays that traverse a much lesser distance in the vertical. Nevertheless, this is an essential peculiarity of acoustic rays traversing in an acoustic waveguide.

The presence of an acoustic waveguide in the ocean helps essentially in the following two ways to simultaneously scan a large ocean volume within a very short time (Behringer et al., 1982): (1) The acoustic rays that are refracted back toward the SOFAR axis before reaching the surface and bottom of the ocean basin lose little energy through the boundaries and, therefore, can be detected over several thousand kilometers; (2) steep rays that sample the entire water column and generally arrive early can be distinguished from flat, late rays that remain nearer the axis, and in this way information can be gathered about the depth dependence of the mesoscale eddy field, which researchers want to detect. Different ray paths give different weights of the water column, and this permits study of vertical eddy structure. Once the travel times of various acoustic rays are obtained (i.e., a direct solution is obtained), the inverse theory is applied to construct a three-dimensional map of the sound-speed field in the scanned ocean basin from *a priori* knowledge of the unperturbed sound-speed field (the reference sound-speed field) in the scanned region.

As part of the Greenland Sea experiment coordinated by the Arctic Ocean Science Board (participating countries included Canada, Denmark, the Federal Republic of Germany, Finland, France, Iceland, Norway, the United Kingdom, and the United States), the Scripps Institute of Oceanography deployed five sets of tomography

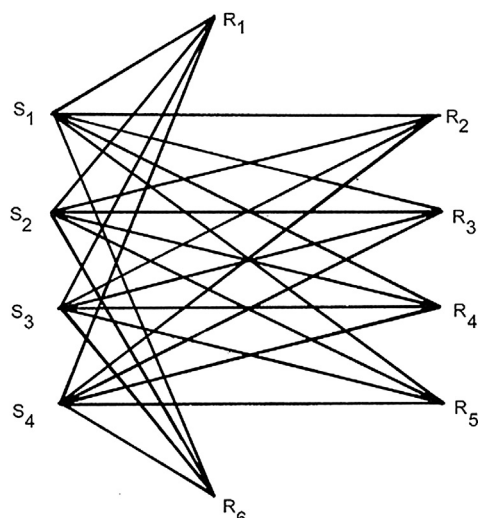


**FIGURE 7.2** Sketch of one of several ways to implement OAT.

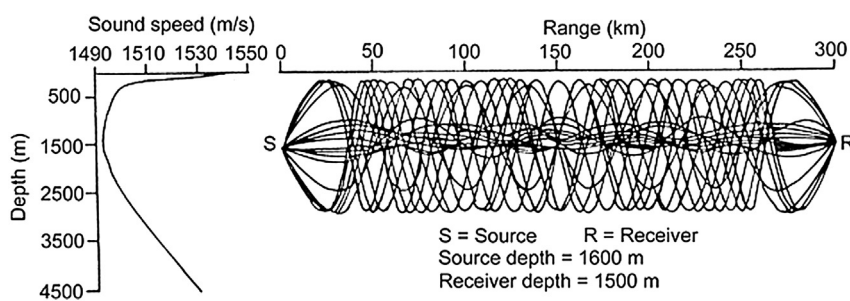


**FIGURE 7.3** Propagation of acoustic rays about the axis of minimum sound speed in a SOFAR channel in the Bay of Bengal. (Source: Kumar et al., 1994.)

instruments on cables moored to the deep-ocean floor at separations of up to 480 kilometers. Each mooring had a transceiver with four receivers at different depths to increase the number of sound-ray paths. The sounds were emitted in 80-second bursts, which took about five minutes to travel the distance between moorings. Over the course of the year-long experiment, the instruments were designed to transmit for a combined total of about 30 hours. This sampling schedule was expected to be adequate because the large-scale ocean phenomena change slowly.

The acoustic transmission loss is both range- and frequency-dependent. For this reason the transmitted signal frequency employed in OAT measurements involving ocean basin-wide distances generally lies in the range 200–400 Hz and usually has a bandwidth of 2–100 Hz. The acoustic wave source is a resonant tube with a length of approximately one-quarter wavelength (in water), driven at one end and open at the other. The acoustic source transducer usually consists of a cylindrical tube of approximately 0.3 m diameter tuned for resonance at the desired transmission frequency. It is driven at the closed end by a flat circular plate of piezoelectric material (lead zirconate titanate) operated at the fundamental tube resonance. The actual tube length is about 10–20 percent greater than one-quarter wavelength due to finite edge effects (Spindel et al., 1977). The efficiency of the source is roughly proportional to the tube cross-sectional area. The acoustic source transducers are essentially of organ pipe design derived from SOFAR float programs and have lengths of approximately a meter. This type of transducer has severely limited bandwidth and is marginally suitable for tomography because a limited bandwidth of the source transducer will limit the sharpness of the processed received signal, thereby limiting the multipath resolution of the receiver. In the early years of tomographic experiments, there were no alternative broadband transducers available.

Ocean acoustic tomography, the process of deploying spatially distributed arrays of underwater sound source-receiver pairs to produce a picture of the inner sea, has advanced from its relative infancy only in the 1980s to a stage on which it is being proven as a reliable measuring device over long stretches of the ocean. The advancement of this process, thought not too long ago to be theoretically implausible, has proven to be a major advancement in oceanographic research.

Because travel time of acoustic signals traversing over a distance of a few 100 km are to be measured with utmost precision, an essential requirement of the transmitted pulse is that it must contain sufficient power (to traverse long distances) and its width must ideally be very small (so that multipath travel times can be adequately resolved). In practice, there is not really much point in going to narrower pulses because the internal waves in the ocean spread and scatter any pulse that is transmitted. If a perfect delta

function is transmitted, the received pulses will still be several milliseconds wide due to internal wave scattering.

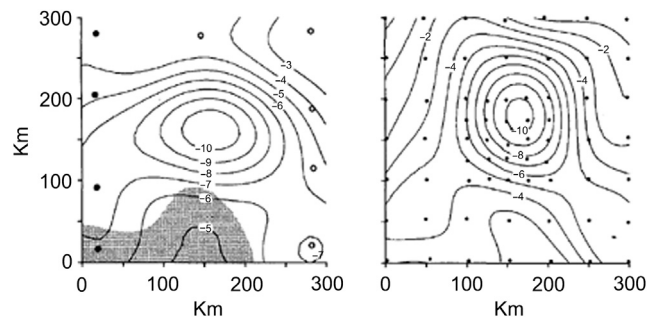
Because these two conflicting requirements are difficult to meet with a narrow pulse, an ingenious technique used in OAT is to transmit a signal (sequence) pattern of large width (so that sufficiently large power can be transmitted) for which the autocorrelation function has a very sharp peak with very low side lobes. The width of the correlation peak establishes the achievable multipath resolution of the system. For many purposes the covariance peak can be regarded as though it had in fact been the transmitted pulse. This pulse-compression technique therefore permits pumping sufficiently high power by the transmitter without sacrificing the multipath resolution of the system. In the acoustic tomography experiment conducted by the Ocean Tomography Group in 1982 (Behringer et al., 1982), a single transmission consisting of 24 consecutive sequences lasted for nearly 192 seconds. Each sequence was a 127-digit maximal-length shift register. Thus transmission of each sequence required 8 seconds, and each pulse was of width of approximately 63 ms. This scheme meant that each transmission was equivalent to the transmission of 127 pulses of 63-ms width at intervals repeated 24 times. The carrier was 224 Hz with a bandwidth of 20 Hz, and the transmitted power level was approximately 14 Watts. At the receiver, the arrival time structure of the multipath field between each source and receiver pairs was obtained by cross-correlating the coherently received incoming signal with a stored replica of the transmitted signal. Some receivers perform this cross-correlation *in situ*; others store signal samples for later onshore processing.

The validity of the interpretation regarding mesoscale eddy fields using OAT techniques depends to a large extent on the precision with which the acoustic pulse travel time is measured. For this reason, an essential requirement of OAT instrumentation is the incorporation of a precision time base. Because the time base derived from quartz crystal oscillators cannot provide the required long-term precision and repeatability, rubidium atomic frequency standards must be used. However, the power requirement of rubidium atomic frequency standards is too high for continuous use in a long-term moored instrumentation such as that of OAT measurements. To meet the stringent requirement of high precision in time-base and low-power consumption, a technique that is usually employed is to switch on the highly stable rubidium atomic frequency standard only periodically (so that power consumption is reduced) and compare the frequency of the considerably less stable (but low power-consuming) crystal oscillator clock frequency with the rubidium standard to get the frequency offset of the crystal oscillator clock. The periodically measured frequency offsets of the crystal oscillator clock are then integrated to yield time corrections.

The receivers are usually equipped with a vertical array of hydrophones separated at a suitable spacing so that the ray inclinations of various multipath arrivals can be computed. The pulse arrival pattern for each ray is predicted using ray theory from *a priori* knowledge of the sound speed in the ocean basin being surveyed. The measured deviations are attributed to perturbations in sound speed along the unperturbed ray paths due to the presence of eddies, meanders, fronts, and so on. The three-dimensional shape and nature of the travel-time perturbations can be obtained from analysis of multipath arrivals from many combinations of acoustic transmitter/receiver pairs in the horizontal array, moored near the axis of the sound channel (approximately 1-km depth). The measured travel-time perturbations are then used to generate the perturbations in the sound-speed pattern in the ocean basin and construct a tomographic picture of the perturbations within the array.

In the first major application of OAT, Cornuelle et al. (1985) chose a substantial ( $300 \text{ km} \times 300 \text{ km}$  square) volume of ocean over four months east of Florida in the western North Atlantic and just south of the region in which the MODE-1 program had been conducted. In this experiment, each source was turned on at one-hour intervals for 24 hours and then shut down for two days so that observations were obtained only every third day. Each time the source was turned on, it transmitted a phase-coded, linear maximal shift register sequence on a 224-Hz carrier (62.5 ms long pulses). Several images of this transmitted sequence were received and averaged by each receiver. Each transmission was cross-correlated with a stored replica of the transmitted sequence, and a best estimate was made (see Spindel, 1979) of the time of arrival of each ray. Two corrections were applied to the raw arrival times. Corrections were made to account for clock drift in the sources and receivers (the procedure is described by Spindel et al., 1982). The second correction comes from changes in mooring position. With acoustic instrumentation mounted 3.5 km above the seafloor, the movement of the instruments in the ambient current field introduces changes in distance between sources and receivers, leading to changes in travel time, which can swamp those due to the mesoscale sound-speed changes. Transponders on the bottom (in a system described by Nowak and Mealy, 1981) determined the temporal variations in the three-dimensional positions of the acoustic instruments.

The goal of the experiment was to make the best possible estimate of the three-dimensional sound-speed field in the ocean volume monitored by the acoustic array. Application of appropriate inversion procedures yielded contours of the sound-speed anomaly (Figure 7.4), which primarily corresponds to water temperature anomaly, revealing a clear *pattern* of eddy structure (an important water circulation and vortex feature) in agreement with the



buoy to decouple the surface buoy's motion from the instruments, has been utilized previously with current meters, which are also sensitive to surface-buoy induced motions. S-tether TOMO is a transfer of this design to acoustic devices, which are even more sensitive to motion effects.

The first trial of the system was in the context of the Thetis experiment in the western Mediterranean, which was a large multinational tomography experiment program aimed at both exploring the oceanography of the western Mediterranean and developing large-scale, long-term monitoring capabilities usable in a wide variety of ocean basins. The mooring was deployed successfully, along with six other moorings, in January 1994, for a 10-month period. However, the telemetry system met with only partial success. Local fishing activity off Mallorca severed the telemetry-link electrical connection between surface buoy and subsurface instruments halfway through the experiment. However, both the surface buoy and subsurface buoy still worked autonomously, which allowed achieving the full scientific objectives.

Functionally, the S-tether mooring has four parts: the surface buoy, the S-tether cable connection from the surface to subsurface float, the subsurface float, and the "standard mooring" down from the subsurface float, which contains the instruments. The surface buoy was a 56-inch diameter, 1,228-pound, syntactic-foam float with a buoyancy of 1,895 pounds. It was designed to be submerged for considerable periods (e.g., covering storm periods) and to reemerge in working order. Its survival depth, based on launch and storm conditions, was rated at 300 meters. The float had a 10-inch × 5-foot-long electronics well that accommodated batteries, a computer, and Argos and GPS units. Externally, the float carried Argos and GPS antennae, solar panels, and recovery aids, all of which were protected from seawater leakage and pressure to survival depth.

The S-tether connection between subsurface buoy and surface buoy was formed by a heavy-jacketed electromechanical cable and a section of compliant rubber stretch hose with an internal electrical conductor path. Through careful distribution of flotation along the electromechanical cable, the cable assumes the shape of a tilted letter S, the stretching of which decouples the surface buoy wave motions from the subsurface buoy. In this configuration, the motions of the tomography source and the hydrophone array are minimized. Under the influence of increasing wind and current drag, the S shape of the cable is gradually straightened out. Thus, even an inclined, linear path provides considerable cushioning from the surface buoy's motion.

The Webb Research Corporation (Falmouth, Massachusetts) tomography transceiver, which was positioned 50 meters below the subsurface float, consisted of a 400-Hz organ pipe source, a four-element hydrophone array, internal battery and electronics, and an external mooring

motion navigator. This instrument was placed relatively near the ocean surface to take advantage of the upward refracting acoustic propagation conditions (surface sound channel) peculiar to the Mediterranean. The equipment below the transceiver included temperature sensors, an Aanderaa Instruments (Bergen, Norway) current meter, a Benthos Inc. (North Falmouth, Massachusetts) acoustic release, and a 6,000-pound anchor.

To transmit at low power and with high efficiency, the acoustic pulses are actually sent out as extended signals (pseudo-random noise, FM sweeps, etc.) that are replica correlated at the receiver to recreate the sharp-pulse multipath structure.

Additionally, we also need acoustic navigation data, tomography-receiver "housekeeping" data, ambient noise data, GPS position data, and (very important) internal instrument clock versus GPS clock data (very accurate clocks are necessary in tomography). Unaccounted-for clock drift is akin to an ocean travel-time signal, causing error in the estimates of oceanic water temperature and current. One of the big advantages of having a surface buoy is the access to a GPS clock.

Digital communications between the transceiver and surface buoy processors were implemented with a low-power, 1,200-baud FSK modem using two conductors. A simple communication protocol based on the oceanographic standard serial ASCII instrumentation loop (SAIL) was implemented to permit the processors in the transceiver and surface buoy to interact and communicate.

Real-time data telemetry was accomplished by transmitting selected, processed tomography and engineering values via the Argos data collection system. To maximize data throughput, a Seimac Ltd. (Dartmouth, Nova Scotia, Canada) PTT was configured with four IDs under software control, each transmitting four 32-byte multiplex packets. In this way it was possible to transmit 512 bytes of data in about 800 seconds, a time comparable to a satellite pass. By updating the buffer twice per day, a total of 1,024 new bytes of data were telemetered daily. Each data buffer was transmitted 54 times, virtually ensuring that each of the 16 data packets would be received at least once. A checksum was used in each transmission to confirm error-free status. The transmitted data consisted of acoustic correlates and times (tomography results), acoustic navigation data, tomography-receiver housekeeping data along with ambient noise data, time offset (internal clock versus GPS clock), and GPS data. With the advent of high-bandwidth satellite systems (such as the Iridium system), high data rates have become possible. Incorporating such schemes, the thorniest problems in using telemetry systems for high-density data reporting have become past history.

With more and more importance having been attached to acoustic tomography, serious attempts have been made to develop better transducers and the related interfacing

instrumentation in place of those borrowed from the SOFAR float era. Because the hitherto existing instruments made by Woods Hole, Webb Research, and the Institute Français de Recherche pour l'Exploitation de la Mer (IFREMER) were not adapted to basin-scale studies (about 1,000 kilometers), in 1994 IFREMER launched the development of a new modular instrumentation for mesoscale OAT measurements. The new autonomous instrument consists of a wideband unlimited-depth acoustic source (Gac et al., 1999) developed and commercialized by ERAMER (Toulon, France), a high-efficiency class-D power amplifier, a programmable multifunction receiver, a long-baseline positioning system, and a low-power, high-stability clock.

In view of the requirement for high-efficiency, low-frequency transducers for operation at great depths, studies conducted in collaboration with the Centre Militaire d'Oceanographie (CMO; Brest, France) indicated that the Janus-Helmholtz technology was the best candidate for basin-scale experiments. For precise measurement of the ocean impulse response, OAT requires a low-frequency acoustic source with a large bandwidth (high time-resolution) and an energetic output sound level. Janus-Helmholtz transducer technology was well suited to long-range OAT applications. With a working central frequency of 400 Hz, 600-km ranges were expected for the initial development. In a simultaneous attempt, a 1-gigabyte storage capacity autonomous receiver capable of operation under various frequency bands was also developed in collaboration with ORCA Instrumentation (Brest, France). Fully compatible with the acoustic source, this receiver system was found to be usable for standard OAT experiments. The new instrument consisted of a 250-Hz Janus-Helmholtz acoustic source, a high-power transmitter associated with many acoustic-processing signal functions, a programmable multifunction acoustical receiver, and a processor with a 1-gigabyte storage capacity.

With very good stability over a large operating temperature range, this new instrument detected and transmitted low-frequency acoustic waves in great water depth. To separate different rays' travel time, the time resolution must be at least 10 milliseconds. Ambient noise in the ocean is a natural limit to the precision that can be attained, but other kinds of effects, such as internal waves scattering and ray interference, would decrease the measurement accuracy. Optimization of the transmit power and the frequency resolution, which define the working characteristic of the transmitter, was found to be the most important criterion in designing and building a Janus-Helmholtz transducer for OAT requirements. The transducer was designed to match, with maximum efficiency, the output level in order to yield a flat bandwidth corresponding to high time resolution. The updated instrument was developed to fulfill the constraints of reliability, low power consumption, and low cost.

The low-frequency Janus-Helmholtz acoustic source (JHAS) is made up of a piezoelectric ceramic stack inserted between two similar head masses. This structure, called a *Janus driver*, is mounted inside a vented cylindrical housing, and the decoupling between head masses and housing is provided by a very thin slit. A fluid with a low-compressibility modulus is inserted inside the cavity in order to satisfy the Helmholtz resonance condition to work at low frequencies and to have a free-flooded device. Because of the coupling of the two resonances, a wide frequency band is available. According to Gac et al. (1999), two frequency bands are usable for OAT applications:

- One between both resonances in order to have a large bandwidth with almost constant impedance values and to be independent of hydrostatic pressure (this was verified from deep-sea measurements in the Mediterranean Sea)
- Another around the second resonance in order to have large transmitting voltage response (TVR) values with high electroacoustic efficiency, allowing small voltage values even if frequency is higher than in the first case

It was found that a working frequency band located between both resonances (frequency bands located around 250 and 400 Hz) was a better way to fulfill bandwidth requirements and to have a constant sound level at any depth, but an improvement of the electrical behavior was then necessary. Due to the length of the ceramic stacks, it was not possible to strongly modify the parallel capacitance ( $C_p$ ) of the JHAS. The only way to optimize the electrical Q-factor and to minimize the power consumption was to have a better coupling between both resonances, which implies an increase of the TVR values in this frequency band (i.e., a decrease of the voltage values) and a decrease of the parallel resistance values ( $R_p$ ). Headmass shape and the opening between cylindrical housings were then modified (ATILA finite-element modeling). Because these modifications led to a frequency shift, the length of the driver had been extended. The JHAS TVR was improved: A 7-dB gain was obtained between the resonances, the electrical Q-factor was halved in the working frequency band, and the electroacoustic efficiency was improved. Thanks to the use of more fluid inside the cavity, the in-water transducer weight remained unchanged. A study of the impedance-matching circuit revealed that sound level and bandwidth requirements to reach 1,000 kilometers ranges in the ocean basin with enough time resolution (maximum sound level equaling 190 dB with a 70-Hz bandwidth) could be satisfied with a 1,500-volt-ampere class-D power amplifier. The new transducer and power amplifier were reportedly nearing completion.

The whole system (i.e., transducer and the electronics interface) was proved during the Cambios oceanographic expedition in the Atlantic at a 600-meter depth. The various

time delays can be distinguished according to the different travel paths.

## 7.2. TWO-WAY TOMOGRAPHY (RECIPROCAL TOMOGRAPHY)

Having succeeded in making of three-dimensional, time-evolving map of large-scale circulation features (e.g., gyres), the next phase was to test *reciprocal tomography*. Reciprocal tomography was expected to be a significant development in oceanographic research. It would improve the ability to make acoustic predictions for several operational purposes.

In a broader sense, reciprocal tomography is indicative of oceanographers' attempts to overcome the limitations they traditionally have faced. An approach to the problem of remote measurement of large scale oceanic motion using reciprocal acoustic transmission method was advanced by [Stallworth \(1973\)](#) followed by [Rossby \(1975\)](#). The central element of this scheme is that the line integral of fluid velocity along an acoustic ray joining two points in a fluid flow field is proportional to the difference in travel times of two acoustic signals simultaneously transmitted from these two points in opposite directions. Via this method, the effects of ocean currents on acoustic propagation can be separated from the effects of sound speed structure (i.e., influence of seawater temperature, salinity, and depth). Reciprocal acoustic transmissions can, therefore, be used to measure ocean currents. One of the unique advantages in using acoustic techniques to measure large-scale oceanic phenomena is that they enable an integral or spatially averaged measurement. For many purposes it is the spatial averages that are of interest, and these are extremely difficult to obtain over large ocean areas in any other way.

The basic premise of using reciprocal acoustic transmissions to measure ocean-current flow is that a sound pulse traveling with a current is faster than the one traveling against a current. This method has been routinely used by meteorologists as early as the 1960s in acoustic anemometers ([Kaimal, 1980](#)) and later by oceanographers for Eulerian current measurements ([Gyre, 1976](#)). Thus, it is well known that the path-averaged sound speed and water current velocity can be measured separately using the reciprocal transmission method. When the direction of water current  $u$  is taken from station  $S_1$  to  $N_1$ , the travel time of sound propagating from  $S_1$  to  $N_1$  is expressed as:

$$t_1 = \int_{\Gamma} \frac{dr}{c(r) + u(r)} \quad (7.2)$$

Similarly, the travel time in the opposite direction is:

$$t_2 = \int_{\Gamma} \frac{dr}{c(r) - u(r)} \quad (7.3)$$

In Equations 7.2 and 7.3,  $c(r)$  and  $u(r)$  are the sound speed in seawater at rest and water current velocity along the ray path  $\Gamma$ , respectively. In Equations 7.2 and 7.3,  $dr$  is the increment of arc length measured along the acoustic ray, and the path integrals are taken along acoustic rays. It may be noted that the acoustic ray path is assumed to be overlapped for the reciprocal course. When  $c_m$ ,  $u_m$ , and  $R$  are considered as the path-averaged sound speed in seawater at rest, path-averaged water current velocity, and path length, respectively, Equations 7.2 and 7.3 get modified, respectively, as:

$$t_1 = \frac{R}{c_m + u_m} \quad (7.4)$$

and

$$t_2 = \frac{R}{c_m - u_m} \quad (7.5)$$

Equations 7.4 + 7.5 and rearrangement yields:

$$c_m + u_m = \frac{R}{t_1} \quad (7.6)$$

$$c_m - u_m = \frac{R}{t_2} \quad (7.7)$$

Equations 7.6 + 7.7 and rearrangement yields,

$$c_m = \frac{R}{2} \left( \frac{t_1 + t_2}{t_1 t_2} \right) \quad (7.8)$$

Taking into account that  $t_1 \approx t_2 \approx \bar{t}$ ,

$$c_m \approx \frac{R}{\bar{t}} \quad (7.9)$$

Equations 7.6 – 7.7 and rearrangement yields:

$$u_m = \frac{R}{2} \left( \frac{t_2 - t_1}{t_1 t_2} \right) \quad (7.10)$$

Putting  $\Delta t = (t_2 - t_1)$  and taking into account that  $t_1 \approx t_2 \approx \bar{t}$ ,

$$u_m = \frac{R}{2} \left( \frac{\Delta t}{\bar{t} \times \bar{t}} \right) \quad (7.11)$$

Taking into account (see Equation 7.9) that  $\bar{t} = \frac{R}{c_m}$ , Equation 7.11 gets modified as:

$$u_m = \frac{c_m^2}{2R} \Delta t \quad (7.12)$$

An average sound-speed profile of the ocean basin at which the reciprocal acoustic transmissions are carried out, appropriate for the time during which the experiments are conducted, is usually constructed by combining data from a series of expendable bathythermograph (XBT) casts and salinity measurements taken along the lines joining

different moorings of the transceiver array. Measurement of mean flow components along two or more different axes permits estimation of the mean water-current flow vector. In an ocean basin-scale measurement scenario using acoustic techniques, where many pairs of transceivers are usually deployed in a large array, it is possible to estimate the mean water-current flow in an ocean basin using this technique.

As indicated earlier, when the reciprocal acoustic transmission technique is applied for measurement of large-scale oceanic water current flow, the differences in travel times of the oppositely traveling pulses are interpreted in terms of acoustic ray-averaged currents. In the simplest approach, it is assumed that sound speed and water current depend only on the horizontal coordinate along a straight-line ray between a given source-receiver pair. Preliminary investigations by Worcester (1977) suggested that differences in travel times of oppositely traveling pulses can be interpreted in a preliminary manner as ray-averaged currents. Because a number of distinct ray paths with a variety of turning depths exist for each source-receiver pair, and each ray represents a different depth-weighted average of the ocean, the ocean basin currents estimated using this technique represent baroclinic (depth-dependent) spatially averaged current fields. However, methods now exist to estimate basin-scale current fields in several horizontal layers of the ocean depth, which yield barotropic (depth-independent) spatially averaged current fields.

The method employed for generation of acoustic transmission signals and processing of the received signals in the reciprocal acoustic transceivers is similar to those used in acoustic tomography experiments. Before deployment, the source-receiver pairs are usually connected in the same loop for clock synchronization purposes. The transmission signal is usually a pulse stream consisting of period repetitions of a phase-coded linear maximal shift-register pseudo-random sequence. The advantage of such a transmission signal code is that it can be processed at the receiver to yield an output waveform that has minimum side lobes (see Figure 7.5). It has the additional advantage that the processing can be easily implemented on a microprocessor. This scheme enables the signal processing to be performed *in situ* in the instrument itself, thus conserving memory space.

Reciprocal tomography received its first at-sea test in August and September 1983 in a 300-km area below the southern portion of the Gulf Stream. To measure the currents in that area, scientists from Scripps and Woods Hole placed moorings 300 km apart and estimated the inter-mooring travel time differences. The frequency for the source was set at 400 Hz during the test.

In the reciprocal acoustic transmission experiment conducted by Worcester et al. (1985), the transmission signal code consisted of a carrier frequency of 400 Hz. The transmission

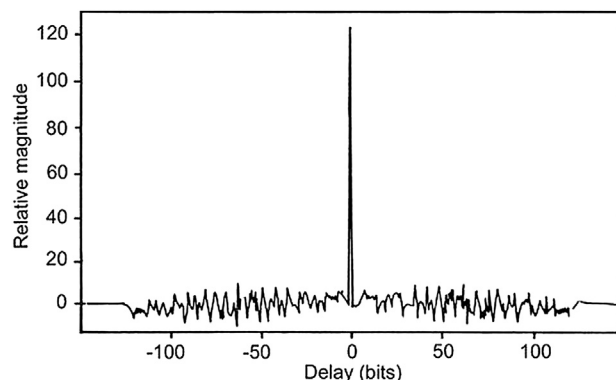


**FIGURE 7.5** Autocorrelation of pseudorandom  $n$ -bit shift register sequences used in reciprocal transmission measurements. The autocorrelation exhibits a triangular peak at zero lag. (Source: Menemenlis and Farmer, 1992, ©American Meteorological Society. Reprinted with permission.)

length was 122.64 seconds, consisting of 24 sequences of 5.11 seconds. The phase-coded 400-Hz digital signal is amplified, usually by a constant-power amplifier. After necessary filtering and impedance matching, the signal is impressed on the drivers of the acoustic transducers. The transducers are resonant tubes, driven by a pair of flat piezoelectric elements inserted at the midpoint of the tube, with an effective length of one-fourth the acoustic wavelength.

In any typical ocean-basin experiment, the expected differential travel time is only a few milliseconds. For this reason it becomes necessary to have a clock with nanosecond precision for the several-month duration of the experiment, requiring an oscillator accurate to better than one part in  $10^{10}$ . In the basin-wide experiment of Worcester et al. (1985), a two-oscillator system was employed to achieve this precision at a reasonable level of power consumption. In this system, a low-power (10-mW) temperature-compensated crystal oscillator (TCXO) ran continuously to drive the clock. A high-power (13-W) rubidium (Rb) atomic frequency standard, which returned to its previous frequency to within two parts in  $10^{10}$  within 10 minutes after power is applied, was turned on at 6-h intervals. The frequency offset between the Rb oscillator, after permitting its warm-up, and the TCXO was used in a feedback circuitry to readjust the TCXO frequency. This feedback technique increased the effective stability of the TCXO by approximately one order of magnitude. Any leftover frequency offset that still existed was measured over a 2-minute interval with a precision of one part in  $10^{10}$  using a phase-comparison technique.

At the receiver section, the signal reception is initiated by the processor at preset times, computed by adding to the programmed source transmit times the expected propagation delay for the nominal range. The received signal is amplified and filtered using a band-pass filter centered at the transmission frequency. Two quadrature components of the

filtered signals, representing the real and imaginary parts of the complex demodulated signal, are generated, low-pass filtered, and then digitized for further “sharp” processing by the microprocessor, to enable detection of successive peaks and their arrival times. Several peaks in the processed received signal arise from multipath signals corresponding to differing acoustic ray paths through the ocean basin.

To resolve all the multipath arrival peaks, including those arriving simultaneously, a vertical array consisting of several hydrophones is required in the receiving transducer assembly. The vertical distance between adjacent hydrophones is maintained at 1.5 times the acoustic wavelength. In this case, processed data from each hydrophone channel are recorded separately so that beams can be formed at any desired angle during post-recovery processing. This will, in addition to improving S/N ratio, permit estimation of the vertical arrival angles of the several acoustic ray paths that impinged on the receiving hydrophone array, thus assisting multipath ray identification by separating simultaneous arrivals from different angles. To perform an inversion of travel-time data, each arrival must be associated with a particular ray path. Furthermore, ray identification is useful in performing inversions to convert travel-time differences to ocean current structure as well. In this sense, use of a vertical array of several hydrophones rather than a single hydrophone assumes special significance. Usually, all signals arrive within  $\pm 15^\circ$  of the horizontal if mooring motion is negligible. Fortunately, mooring motion does not seriously affect the two-way travel times in reciprocal acoustic transmissions (velocity tomography), although mooring-motion correction is most important in the one-way travel times used in acoustic tomographic measurements (density tomography). This is because, in the case of reciprocal transmissions, the differential travel time is directly proportional to the ray-averaged current with respect to the mean motion of the transceivers (Worcester, 1977). One probable source of error in the inversion of differential travel times to obtain currents arises from the influence of current shear in causing the acoustic ray paths to differ with and against a current. Sound pulses traveling in opposite directions, therefore, do not sample precisely the same part of the ocean (Worcester et al., 1985). Fortunately, by virtue of Fermat’s principle, travel time is unchanged to first order in small perturbations in the ray paths. Effects associated with the nonreciprocity of ray paths are expected to be small if the sound-speed gradient and current gradient are comparable.

### 7.3. ACOUSTIC TOMOGRAPHIC MEASUREMENTS FROM STRAITS

Water currents in straits (narrow passages of water connecting two large water bodies such as basins of oceans or marginal seas) are typically highly variable in both the

horizontal and the vertical. Straits potentially provide important observation sites for various applications. For example, the net transports of mass, heat, and salt through such passages give integrals of the fluxes over the interior basin. Alternatively, the flow through a strait may represent a control for interior processes or forcing and thus is of interest for the functioning of the basin or as a boundary condition for modeling studies (Send et al., 2002). The highly variable nature of currents in straits makes it difficult and expensive to obtain reliable, long-term transport observations using point measurements. An adequate current-meter array, for example, typically requires a sequence of current-meter moorings across a strait, spaced closely enough in the horizontal to resolve the cross-strait current scales and with current meters spaced sufficiently densely on each mooring to resolve the vertical scales.

For long-term observations, one would prefer a shore-based observing system. Among those systems, sea-level differences integrate only the surface currents across the section. Electromagnetic (cable) methods (see Chapter 2) seem promising for observing barotropic currents but are subject to some side effects and are not suitable for observing the exchange in two-layer currents. The acoustic transmission method (e.g., transmission from one side of a strait to the other) offers some promise because this method inherently integrates horizontally over the flow and provides information on the flow along the path bounded between the acoustic instruments, without the need to deploy instruments in the interior of a strait. A variety of methods are theoretically possible for the use of acoustics in this context.

It has been found that in the deep ocean, the acoustic arrivals are stable and the received acoustic pulses can be resolved and identified with ray paths. However, acoustic transmission in shallow-water regions such as straits, coastal water bodies, and estuaries is quite different from that in deep oceans. An axis of minimum sound speed exists in deep oceans, but such an axis does not exist in shallow waters, where sound speed typically decreases with depth so that ray paths are refracted downward, and propagation to moderate ranges (of the order of a few kilometers) necessarily involves bottom bounces (De Ferrari and Nguyen, 1986). Further, because of the loss caused by bottom interactions, long-range acoustic transmission in shallow water is not possible. Although long-range acoustic transmission paths in the deep ocean are mostly refracted/reflected (RR) paths, the transmission paths in shallow-water acoustic transmission are usually refracted/bottom-reflected (RBR) paths and surface-reflected bottom-reflected (SRBR) paths. Those arrivals traveling via the SRBR paths suffer high losses due to high-angle interactions with the ocean surface and bottom so that pulse responses are dominated by the RBR arrivals. The earliest arrivals are those that follow the

steepest RBR paths and reach the higher sound-speed region of the upper ocean. The latest arrivals are those that travel along the flattest RBR paths, propagating in the slower sound-speed near-bottom water. These observations indicate that deep-ocean tomography methods may not be successful in shallow-water applications. Deep-ocean tomography inversion techniques require that the individual eigen rays be separable in time, identifiable, and have known paths through the ocean. However, in shallow areas at long ranges, unresolved multipaths will be the rule (Muller et al., 1986).

A major difficulty with acoustic tomographic and reciprocal measurements in shallow water is that multipath interference rapidly changes the pulse shape and phase. Furthermore, acoustic multipath pulse arrivals overlap and form groups. Measurements by Ko et al. (1989) in the Florida Straits showed that these groups are generally not consistent and often cannot be resolved. This means that in shallow water, it is difficult to identify acoustic arrivals with particular ray paths. However, shallow areas are often of great oceanographic interest.

To surmount some of the difficulties associated with long-range acoustic propagation in shallow-water basins and to achieve precision in measurement, one approach is to measure the pulse response of the acoustic channel with high resolution and then attempt to use multipath groupings, correlation methods, or phase information to resolve travel times.

Experiments by De Ferrari and Nguyen (1986) in the Florida Straits indicated that a convenient depth average is associated with those rays forming the late peak, and the arrival time of the late peak is a measurable and consistent feature of the data. The resulting depth average is determined by the source and receiver depths. Thus, information about the depth dependence of current is possible with a single parameter inversion by employing a vertical array of hydrophones. The purpose of having such a hydrophone array in deep-ocean tomographic measurements is to select the acoustic arrivals, but the purpose of such an array in shallow-water acoustic measurements is to select average height of the ray, thus controlling the depth and the extent of averaging the current.

In shallow-water acoustic pulse propagation, the signals arriving earlier than the late pulse generally are less stable and of lower amplitude. Even with longtime averaging, it is difficult to identify characteristic features that can be tracked and used for precise measurement of travel time. However, a consistent feature of the pulse response of a channel is a sharp peak associated with the late-arriving RBR paths. The purpose of averaging several pulse responses is to smooth out interference effects. The stable and sharp cutoff of the late peak is used to align the pulses prior to their averaging. The arrival time of the pulses is estimated using a *threshold cross-time* method, whereby the arrival time of the lagging edge is estimated as the time

when the edge crossed an intensity threshold. This threshold is usually an average of several thresholds, which are 10 dB or more below the maximum intensity of the late peak. The aligned pulse responses are averaged, with the moving window over several records (the *sliding average method*).

Ko et al. (1989) found that the pulse responses lined up very well after being aligned and averaged. Because the time corresponding to the maximum intensity of the peak is an imprecise estimate, the centroid estimation is usually used to estimate the travel time of the arrival peak. The time corresponding to the centroid of the late peak is computed using several points around the maximum value. The time variation for the late peak has been found to be a good indicator of the travel-time variation for the latest, and thus the flattest, near-bottom RBR rays. Details of data analysis methods may be found in De Ferrari and Nguyen (1986).

Suesser (1990) examined the properties of the acoustic environment in the Strait of Gibraltar, with the goal of determining the feasibility of using acoustic remote-sensing methods to monitor temperature and/or current structure there. Subsequently, Elisseeff et al. (1999) reported acoustic tomographic measurement of a coastal front in Haro Strait, British Columbia (Canada). In their experiments, each mooring consisted of 16 receivers, a 1.5-kHz tomographic source, and a 15-kHz communication source (see Figure 7.6). A chain of thermistors was added to two of the four moorings. The moving source used in this study consisted of ship-deployed lightbulbs. The lightbulbs were lowered to a specified depth in a casing apparatus, as shown in Figure 7.7. The shot was then triggered by breaking the bulb at depth using an operator-released lead mass that dropped along the cable from the ship to the casing. Lightbulbs generate a short, reproducible bubble-pulse waveform. The spectral peak of the

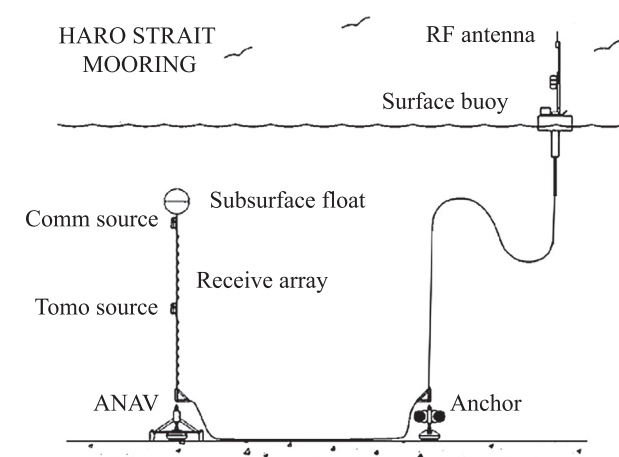


**FIGURE 7.6** Haro Strait acoustic tomographic array mooring design. (Source: Elisseeff et al., 1999.)

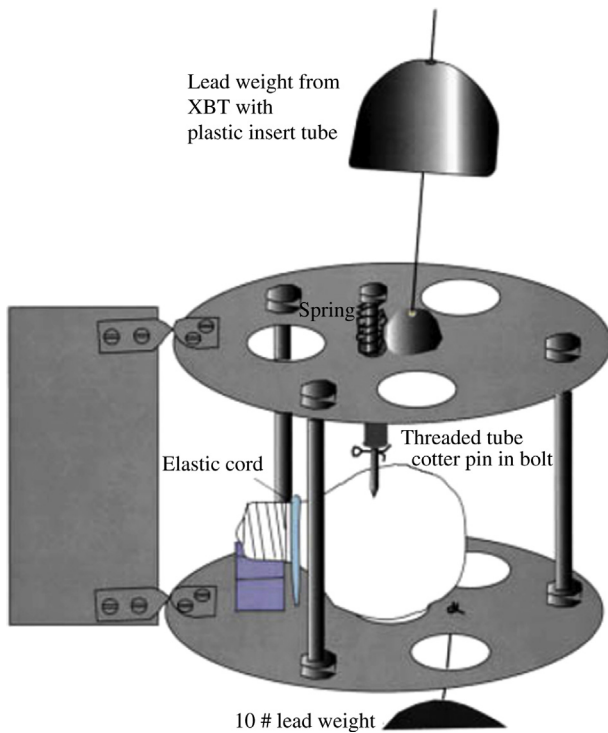


**FIGURE 7.7** Design of moving acoustic source consisting of ship deployed lightbulb lowered to a specified depth in a casing apparatus. The lightbulb generates a short reproducible bubble-pulse waveform (shot) when the bulb is pierced at the specified depth using an operator-released lead mass that is dropped along the cable from the ship to the casing. (Source: *Elisseeff et al.*, 1999.)

lightbulb-generated wideband acoustic signals is typically about 500 Hz at a depth of 50 m, with a 3-dB bandwidth of approximately 300 Hz. Although there is significant spectral content to several kHz, the band was limited in this experiment by the relatively low sampling frequency of 1,750 Hz. Source locations were obtained using differential GPS data.

The four 16-element vertical acoustic line arrays were moored south of Stuart Island (see Figure 7.8) around the location of a coastal front driven by estuarine and tidal forcing. Four non-acoustic moorings were also deployed along the Haro Strait channel. Local temperature, salinity, current magnitude, and current direction were recorded by these moorings at discrete depths. These shots were recorded on all the moorings and were all deployed within a time period of approximately 90 minutes. Source depths ranged from 30 to 70 m. Source levels were approximately 160 to 170 dB//1  $\mu$ Pa. The acoustic data acquired on each receiver array were sent back to shore via a surface radio link at a rate of 35 kbauds. Various acoustic signals were transmitted from array to array and from the moving source to the arrays over a period of five weeks. Tomographic signals were transmitted over a wide-frequency band (150 Hz to 15 kHz). The novelty of the Haro Strait

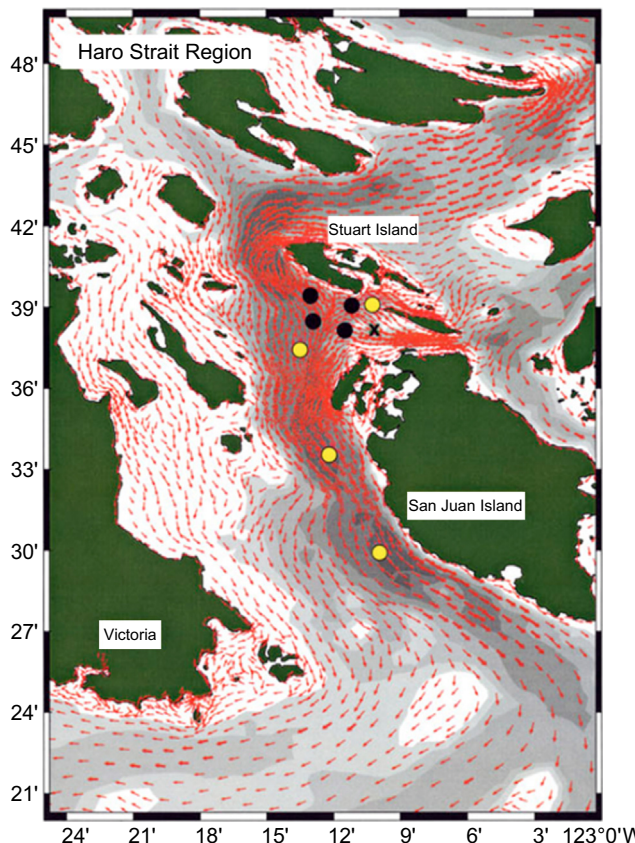


**FIGURE 7.8** Topographic map of Haro Strait region with predicted ebb tide currents during tomographic experiment. Tomographic arrays (black circles) were deployed to investigate the front south of Stuart Island. Current meter moorings (yellow circles) and a meteorological surface buoy (black cross) were used to help clarify the large-scale circulation. (Source: *Elisseeff et al.*, 1999.)

dataset resides in its unusual tomographic features: Ranges are short (less than 3 km), sound-speed perturbations are small (2 to 3 m/s), and currents are relatively strong (3.5 kts).

Individual acoustic time series were match-filtered using a single arrival as a substitute for the actual source signal. Absolute timing was provided by an acoustic acquisition system described by *Grund et al.* (1997). The magnitude of the matched-filter output was then low-pass-filtered using a zero-phase third-order Butterworth filter with a cutoff frequency of 500 Hz. Direct and surface ray arrival times were subsequently measured by identification of the corresponding local maxima of the filtered time series. Acoustic sensor localization was carried out by minimizing the mean-square difference between the measured arrival times and the arrival times predicted using a sensor model.

Raw temperature, salinity, and water-current time series were measured at the mooring sites at a frequency of 12 samples per hour. Sound speed,  $C$  (m/s), was estimated

from water temperature  $T$  ( $^{\circ}\text{C}$ ), salinity  $S$  (psu), and depth  $D$  (m) using Mackenzie's formula (Mackenzie, 1981):

$$\begin{aligned} C = & 1448.96 + 4.591T - 5.304 \times 10^{-2}T^2 + 2.374 \\ & \times 10^{-4}T^3 + 1.304(S - 35) + 1.630 \times 10^{-2}D \\ & + 1.675 \times 10^{-7}D^2 - 1.025 \times 10^{-2}T(S - 35) \\ & - 7.139 \times 10^{-13}TD^3 \end{aligned} \quad (7.13)$$

Individual samples were grouped by 50-min bins and averaged. Standard deviations were found to be between 6 and 13 cm/s for the current field and between 1 and 25 cm/s for the sound-speed field.

To combine heterogeneous datasets, a variety of observation models is required. Acoustic sensor displacements are accounted for by a sensor model. This model relates acoustic sensor displacements to array design parameters and local current magnitude at the array. The water-current model provides predictions of the tidal current field at any point in the observed region. The acoustic model relates sound speed to acoustic travel times. Statistical field estimates provide *a priori* information on the actual field estimates. A *posteriori* information on water current is provided by local water-current measurements and acoustic sensor displacements. A *posteriori* sound-speed information is provided by local sound-speed measurements and acoustic tomographic data. In a first stage, an estimate of the oceanic water current field is computed by objective analysis of the available current data (Carter and Robinson, 1987). The water-current estimate is then externally melded with the tidal-current model prediction following a standard data assimilation procedure. The sound-speed field is then objectively analyzed using range-averaged acoustic tomographic estimates and local nonacoustic data.

Elisseeff et al. (1999) combined two types of information in the estimation of the sound-speed field:

1. Point measurements of sound speed at the nonacoustic moorings
2. Acoustic travel times measured at the acoustic moorings

First, the acoustic travel times are used to estimate range-averaged sound-speed profiles and their error covariance along the available acoustic transmission tracks. These sound-speed profiles are then merged with the point measurements and interpolated to yield an estimate of the sound-speed field.

Lightbulb-generated low-frequency wideband acoustic signal transmissions and the received acoustic dataset gathered in Haro Strait in June 1996 were used in conjunction with local nonacoustic measurements in order to image the three-dimensional sound-speed and water-current fields

within the water mass of approximately  $3\text{ km} \times 3\text{ km} \times 200\text{ m}$  enclosed by a group of moored arrays. A fast and robust inversion algorithm combining linear techniques previously used in deep-ocean tomography and oceanographic data assimilation was developed by Elisseeff et al. (1999), yielding the real-time oceanic field estimates required in the context of acoustically driven rapid environmental assessment. The use of data melding and data assimilation techniques allowed them to resolve, to some extent, the current/sound-speed ambiguity inherent to any nonreciprocal acoustic transmission. In addition, the combined use of integral and local data led to a significant decrease of the field estimate uncertainty while maintaining coverage of the area that was not achievable by nonacoustic means.

## 7.4. COASTAL ACOUSTIC TOMOGRAPHY

As mentioned earlier, most acoustic oceanographers have focused their major interest on the open ocean. Thus, in contrast to the frequent use of reciprocal transmission techniques in the open ocean, no reciprocal transmission experiment has been performed in the coastal ocean for quite some time since the development of OAT techniques. The major reason for this inaction has been a plethora of technical problems associated with the complicated nature of sound transmission in shallow water bodies. In the coastal ocean, long-term measurements of currents has often been prohibited by heavy ship traffic and fishing activities. Despite such difficulties, Zheng et al. (1997) designed and developed a reciprocal sound transmission system to measure currents over a long-term basis in a Japan coastal sea with heavy ship traffic and fishing activities. They successfully demonstrated that reciprocal sound transmission is applicable to water-current velocity measurement in the inland sea with heavy ship traffic and fishing activities. It is well accepted now that, especially around Japan, sound transmission techniques may be a possible method to realize a long-term monitoring of through-flows in coastal channels.

The reciprocal transmission system designed by Zheng et al. (1997) was composed of two stations located on the opposite sides of the coastal channel, where measurements were desired. Both stations were equipped with a transmitter, hydrophone, and GPS receiver. The GPS receiver was used not only to locate the stations but also to synchronize their clocks. In this system, 1-Hz and 1-kHz signals from the GPS receiver were used for timing of the system. Starting signals of transmission were sent by detection of local time and 1-Hz pulse signals. Reception of signals was initiated by counting a delay time with 1-Hz and 1-kHz pulse signals. The transmission clock ( $\text{CLK}_t$ ) and the coherent carrier signals for demodulations were

synchronously locked by a phase-locked loop (PLL) circuit using 1-kHz signals from the GPS. As a result, the timing of transmission and reception for each ping was controlled to an accuracy of 0.1  $\mu\text{s}$ . Transmission signals, a carrier of frequency 10.6 kHz modulated by M-sequence (briefly described in the following paragraph), were generated by driving the data written in programmable read-only memory (PROM). First the received signals were processed through a preamplifier, band-pass filter, and amplifier. Next they were demodulated by the multiplier and low-pass filter using the coherent carriers and divided into in-phase (I) and quadrature (Q) components. Finally, the analog signals were digitized by an A/D converter and recorded on the hard disk of a microcomputer.

Coastal oceans frequently suffer from a noisy acoustic environment due mainly to ship traffic. Consequently, a special method of sound transmission and signal processing was needed. A method for extracting the received signals from noisy data is the use of M-sequence and the cross-correlation of received signals with it. The *M-sequence* is a kind of pseudo-random signal by which a phase shift of  $\pi$  radians in the carrier is generated with irregular time intervals (Okujima and Ohtsuki, 1981). Zheng et al. (1997) have reported a typical example of M-sequence, with time series of the original signal and its autocorrelation coefficient. There are two kinds of time scales in the M-sequence, the period ( $T_p$ ) and the width of one digit ( $T_r$ ). After the autocorrelation procedure, the S/N ratio can be improved by  $(2n - 1)$  times for the M-sequence of  $n^{\text{th}}$  order. Zheng et al. (1997) nomenclatured the improved rate of the S/N ratio as *processing gain* ( $G_p$ ). The travel time of an acoustic ray propagating between two stations is determined as a peak position of the autocorrelation coefficient of triangular shape in an ideal case without ambient noise. When two acoustic rays with the same intensity arrive successively within a short interval of time, the autocorrelation pattern for the rays is overlapped. For the travel-time difference ( $\Delta t$ ) less than  $T_r$ , we lose the individual peaks that each autocorrelation pattern possesses. According to Zheng et al. (1997),  $T_r$  can be termed as the *time resolution* of the system for multiple arrivals. In the case of two acoustic rays with different intensities, individual correlation peaks may be detectable even for the overlapped arrival because of the difference of the peak height. Smaller  $T_r$  is required for a better resolution of time but needs a transmitter with a wide range of frequency response. In the system designed by Zheng et al. (1997), the order of M-sequence is set to 10 for increasing the S/N ratio by  $2^{10} - 1$  (30.1 dB), and  $T_r$  is taken as three times the period of the carrier. This condition puts the frequency range of transmitted signals into  $10.6 \pm 3.53$  kHz and matches with the frequency response of the transmitter. As a result,  $T_r$  and  $T_p$  are given as 0.283 ms and 0.290 s, respectively.

A sound level ( $SL$ ) at the transmitter is set to about 190 dB (relative to 1  $\mu\text{Pa}$  at 1 m). The propagation loss ( $PL$ ) of sound waves against the range ( $R$ ) is expressed by (Urick, 1983):

$$PL = 20 \log R + \alpha R + L_0, \quad (7.14)$$

where the first, second, and third terms on the right-hand side of Equation 7.14 correspond to the spreading, absorption, and other losses (directivity, reflection, interference, etc.), respectively. The absorption coefficient  $\alpha$  is set at 0.00132 dB/m at 10.6 kHz. In Equation 7.14,  $R$  is  $m$  in dimension. The received sound level ( $RL$ ) at the hydrophone is given from the sonar equation as:

$$RL = SL - PL = SL - 20 \log R - \alpha R - L_0. \quad (7.15)$$

The signal-to-noise ratio ( $S/N)_R$  of received signals obeys the following equation:

$$\begin{aligned} (S/N)_R &= RL + G_p - N_a \\ &= SL - 20 \log R - \alpha R - L_0 + G_p - N_a, \end{aligned} \quad (7.16)$$

where  $G_p$  is the processing gain due to the use of M-sequence and taken to be 30.1 dB, and  $N_a$  is the total level of the noise composed of the ambient noise ( $NL$ ) and the system noise. In the Seto Inland Sea,  $NL$  is mainly caused by ship traffic, and within the operating frequency range of the hydrophone and the receiving circuit was estimated as 85 dB, greater by 30 dB than that in the open ocean (Wenz, 1962). The total level of the noise ( $N_a$ ) reduces to about 100 dB in consideration of system noise. Setting  $L_0 = 10$  dB for direct rays (not reflected at both the surface and bottom), Zheng et al. (1997) obtained  $RL = 97.36$  dB and  $(S/N)_R = 27.46$  dB. For the sound transmission system used by Zheng et al. (1997), the accuracy of travel-time measurement depends on  $T_r$  and  $(S/N)_R$  and is expressed by (Munk and Wunsch, 1979) as:

$$T_a = \frac{T_r}{\sqrt{10(S/N)_R/10}} = 12.0 \mu\text{s}, \quad (7.17)$$

where  $T_r = 0.283$  ms.

Zheng et al. (1997) carried out a reciprocal sound transmission experiment on July 14, 1995, in the Seto Inland Sea, Japan. The peculiarity of this region is that a pair of vortices is induced by an eastward tidal jet coming out from the Neko Seto channel (Takasugi et al., 1994). Accordingly, the possibility of a clockwise vortex appearing on the proposed sound transmission line was expected when the direction of tidal current turns from the east to west and moves slowly to the southwest in the growth of westward tidal flow. Based on this realization, the sound transmission experiment of Zheng et al. (1997) was planned to start immediately after the tidal current changed its direction from east to west. They expected that water and flow properties in the tidal vortex are homogenized

(i.e., well mixed) in the entire depth because the diameter of the vortex of about 4 km is much larger than water depths at the observation site. The main purpose of this study was to develop a reciprocal sound transmission system of a 10-km scale applicable to the coastal ocean with severe ambient noise due mainly to ship traffic.

The system was composed of two stations spaced with a distance of 5.7 km on both sides of a channel in the Seto Inland Sea. Each station was equipped with a transmitter, hydrophone, and GPS receiver. The transmission line of length 5.7 km between the stations  $N_2$  and  $S_2$  was taken to cross a small coastal channel surrounded by Honshu (the biggest main island of Japan) and Kami-Kamagari Island. The bottom slopes steeply down near these two stations and maintains a constant depth of about 70 m in the remaining region except for a bank at the northern part of the line. The subsurface system equipped with a transmitter and hydrophone was suspended down in water through an aluminum shaft from a fishing boat anchored at the stations  $N_2$  and  $S_2$ , the depths of which were about 20 m. The transmitter and hydrophone were installed at 5 m and 5.5 m, respectively. A directional transmitter and an omnidirectional hydrophone were used.

As an example, for  $R = 5.7$  km and  $c = 1,500$  m/s, measurement of the seawater current velocity of 1 cm/s requires that the acoustic travel-time difference ( $\Delta t$ ) be measured with an accuracy of 50.67  $\mu$ s. Taking this into account, a pulsed signal of time width 0.29 s corresponding to a period of the M-sequence was transmitted every minute from the stations  $N_2$  and  $S_2$  with a time difference of 30 s between the two stations. The recording of received signals started in a delay time of 3.75 s from the transmission and continued for 0.983 s. The sampling time of the A/D converter was 20  $\mu$ s. In this experiment, one-period M-sequence was used as a transmitted signal. The one-period M-sequence method is known to make spurious correlation peaks on both sides of the true correlation peak, which corresponds to an arrival ray (Okujima and Ohtsuki, 1981). Zheng et al. (1997) estimated the level of the spurious peaks to be 14.4 dB lower than that of the true peak. This means that no problem takes place in this study, which deals with only a first arrival ray.

The third boat was operated for ADCP and CTD measurements, which proceeded in parallel with the sound transmission experiment. The RD Instruments 300-kHz broadband ADCP was installed at 1 m below the surface by an aluminum frame mounted on the side of the boat. The bin length and sampling time were set to 2 m and 12 s, respectively. The bottom tracking bins also profiled bottom topography. CTD casts (Alec Electric Corporation AST-200) were done over the whole depth at seven stations, including the stations  $N_2$  and  $S_2$ . The correlated signals possessed small peaks behind the first correlation peak, implying the successive arrival of signals. The original

signals also showed a remarkable change before and after the first correlation peak.

Combination of measurements of water temperature, salinity, and flow velocity between stations  $C_5$  and  $C_7$  enabled detection of the anticipated clockwise vortex. Southwestward movement of the vortex was well traced with a sequence of positions where minima of  $u$  or zero velocities of  $v$  occurred. The correct feature of such moving vortices may be a difficult target to be measured by the slowly moving ship equipped with an ADCP.

Yamoaka et al. (2002) made continuous effort since 1994 to construct a cost-effective multiple set of coastal acoustic tomography (CAT) systems. At the beginning of March 1999, five sets of the moored-type CATs were constructed, and they have been applied to measure vortex structures in the Neko-Seto Channel of the Seto Inland Sea with strong tidal currents. Inverse analysis has been applied for reconstructing horizontal current fields from the travel-time difference data. The internal host computer controls all the clock, transmission, and receiving circuits. Timing of sound transmission and receiving is coherently synchronized with an accuracy of 0.5- $\mu$ s by GPS pulse signals. The time base module (a SeaSCAN precise crystal clock) becomes a system clock when the GPS signals are interrupted because of unexpected problems. Temperature and salinity are well homogenized due to strong tidal mixing over the entire observation region except the upper 5-m layer. In the upper 5-m layer, the sound speed follows the temperature profile, and below the surface layer it increases with the pressure, forming an adiabatic profile.

Acoustic signals are transmitted every 5 min by an omnidirectional transmitter (ITC2011/ITC2040) with horizontally directed beams of  $\pm 30^\circ$ . A Gold sequence of the tenth order, which is a kind of pseudo-random sequence, is used for phase modulation of signal transmission (Simon et al., 1994). The Gold sequence is constructed by a product of the preferred pair of M-sequence codes of tenth order with the optimal cross-correlation property, maintaining the original cross-correlation property of the M-sequence. The M-sequence of tenth order has only three sets of the optimal cross-correlation property, whereas the Gold sequence of the same order can generate 1,025 optimal sets. This advantage enables CATs to carry out multistation tomography with a simultaneous transmission. Transmission signals are received by a hydrophone (Benthos AQ-1). The received signals are preamplified and divided into sine and cosine channels for a complex demodulation. After the signals are low-pass-filtered and A/D converted, the digital signal processor (DSP) TMS320c548 promptly calculates the cross-correlation between the processed signal and the transmission codes that are used in the transmission and stores the results to the hard disk. In the observation region, a depth-averaged water-current velocity field can be

reconstructed through the inverse analysis of travel-time difference data for all station pairs in the tomography array.

The first coastal acoustic tomography experiment was carried out on March 2–3, 1999, in the Neko-Seto Channel of the Seto Inland Sea, Japan. Several crowded shipping routes are distributed throughout most parts of the Neko-Seto Channel. Five sets of CATs were placed at stations from S1 to S5 in the periphery of the Neko-Seto Channel. The distance between two neighboring stations ranges from 1.9 to 5.5 km. In this region, the tidal current is directed eastward at the flood tide and westward at the ebb tide. The bottom topography, which is characterized by sand banks and troughs, is formed by the action of a pair of tidal vortices induced by a strong eastward tidal jet flushed out from the narrow western inlet (Takasugi et al., 1994). Previous research has determined that the tidal vortices develop as the eastward current is strengthened and they reach a maximum size of about 2.5 km two hours after the strongest eastward current. The vortices move toward the narrow inlet at the incipient phase of the westward current and diminish rapidly with increasing westward currents.

The rays of sound propagation are simulated by the ray-tracing method in which the CTD data are used to specify the reference sound speed. The direct rays, which have no interaction with the sea surface and bottom, pass the upper 20-m layer, where the near-surface duct exists. The computed travel times for all the direct rays have a scatter of 0.4 ms, which is less than the one-digit width (0.54 ms) of a Gold sequence. Thus the arrivals cannot be resolved, and the first arrival peak is composed of multiple direct rays.

Received signals for each station are cross-correlated with the same Gold sequence code as that used in the transmission signal. Travel-time difference data for the first arrival peak determined in the correlation peaks is used as data in the inverse analysis. In fact, the travel-time measurement is affected by the accuracy of clock timing and the horizontal movement of the transmitter and hydrophone. When the accurate clock timing is available, the relative error of current velocity measurement ( $\Delta u/u_m$ ) may be formulated by  $\Delta u/u_m \approx \Delta L/L$ , using the relative-positioning error ( $\Delta L/L$ ), where  $u_m$  and  $L$  are the range-averaged current velocity and the station-to-station range, respectively (Zheng et al., 1997). It would be noteworthy to keep in mind that the relative error of current velocity is only 0.2 percent of the observed current velocity for observation range 5 km and positioning error 10 m.

The travel-time difference ( $\Delta t$ ) may be converted into the range-averaged current velocity ( $u_m$ ) using Equation 7.12, where  $R$  is the station-to-station range and  $c_m$  the range-averaged sound speed. It has been noted that the oscillation due to the semidiurnal tide is featured for several transmission lines.

In the studies reported by Yamoaka et al. (2002), the inverse analysis was performed only for the first arrival

peaks estimated by the ray theory, because the identification of bottom reflected/scattered rays was much more difficult due to the interference of sound waves in shallow water. The high-frequency variability of current velocity was found to have been considerably enhanced with decreasing station-to-station ranges. This high-frequency variability expressed by the standard deviation from the 30-min mean was proposed as a good index of the error bar in the velocity measurement. The relative magnitude of direct to scattered rays in received signals was found to increase with increasing station-to-station ranges because the intensity of scattered rays is more rapidly damped due to bottom bouncing. That was why the high-frequency variability of travel-time difference was found to have been so large for the station pairs with much shorter station-to-station ranges.

It is encouraging to note that the CAT system composed of five moored acoustic stations could reveal the horizontal structure and the temporal variations of the tidal vortices in straits. Although an advanced technique of data analysis is expected, the overall process of growth, translation, and decay of the tidal vortex pair was fairly reconstructed by the conventional inversion method. Based on the studies of Yamoaka et al. (2002), it was found that for the same number of moorings, the spatial resolution of the tomography is considerably improved compared with the conventional point measurement technique. Whereas the spatial resolution for the conventional technique can be improved by increasing the number of moorings, the instrumentation cost is correspondingly increased with the number of moorings. On the other hand, whereas the mapping of coastal surface currents can be performed by the HF radar systems, the acoustic tomography measures depth-averaged currents with the future extension to the vertical profile measurement of current. In the Seto-Inland Sea region, because of the development of residential and industrial areas, it may be difficult to find sufficient shore space for locating the array of antennae needed by HF radar. In contrast, CAT, operated by multiple sets of compact mooring stations and placed near the shore, can be a practically feasible system with more flexibility and potential ability than HF radar.

In the Neko-Seto Channel, the mooring observation has been strictly prohibited by the Japan Maritime Safety Agency, except for the near-shore region, because of the risk of shipping accidents. Limited information on the vortex generation in the Neko-Seto Channel may be provided by shipboard ADCP operating along several lines covering the observation region. However, the rapid processes of growth, transition, and decay of the tidal vortices were first measured by Yamoaka et al. (2002) using an acoustic tomography technique. It is hoped that in the near future, the tomography system may make further progress, with new instruments to measure the phenomena

of strong tidal mixing and dissipation in the Neko-Seto Channel and around a huge number of islands located in the Seto Inland Sea without disturbing marine traffic. When this happens, the sophisticated tidal model of the Seto Inland Sea, including the Neko-Seto Channel, will be fully operational. At this stage, real-time data telemetry via satellite or mobile phone is desired for predicting current variability in combination with the ocean model. It was also proposed that a long-term operation at shorter intervals could be conducted by putting solar panels on a surface buoy.

From the preceding examples of acoustic tomographic experiments, it can be expected that an increase in the number of tomographic source-receiver pairs makes it possible to achieve more detailed mapping of current fields in the coastal seas. Yamaguchi et al. (2005) applied multiple CAT systems to map tidal current structures generated at the Hayatomono-Seto of the Kanmon Strait. In Japan, most of the CAT measurements have been carried out in this strait, which is a narrow passage with a width of 1–2 km and a length of about 28 km. This strait is located in the Sea of Japan and it is famous, not only as an important shipping traffic route to China and Korea but also as a dangerous passage with quite strong tidal current exceeding 5 m/s at the narrowest point.

Since the time of tidal current measurements in this strait with the use of drifting floats tracked by many small boats in the 1940s, more comprehensive measurements have been prohibited due to crowded shipping traffic. Although the maximum current and the vertical section structure of current across several transects were well observed with the use of repeat shipboard ADCP measurements, information on the horizontal structure of current and its temporal variation in this strait was rather scarce. The temporal change of volume transport across the strait was also poorly known. Except for continuous measurement of currents routinely performed at one station near the Kanmon Bridge (the narrowest point) by the Japan Coast Guard using an upward-looking, bottom-mounted ADCP and the collected data made available to the public in the form of tidal current charts published by the Japan Coast Guard (1994), no more information on the current structure and its spatial variability was available. This was the reason that primarily stimulated the oceanographic researchers to undertake CAT experiments in this strait.

We have noted that Yamaoka et al. (2002) challengingly measured the two-dimensional tidal vortex fields in the Neko-Seto Channel of the Seto Inland Sea using CAT experiments. It has been seen that the overall features of the tidal vortex fields were reasonably well reconstructed through inverse analysis in which travel-time differences obtained for the pairs of five acoustic stations were used as input data. However, the influences of the open boundary conditions and the complex coastline on current fields were

difficult to include in the inversion. A coupling of the tomography data with the ocean model was expected to satisfy the dynamic constraints of current fields and the boundary conditions.

Although CAT technology was found to be a practical means for integrated measurement of coastal currents and their circulation structures, the application of this technology in the Japanese Inland Sea was beset with a couple of practical issues that needed to be resolved. In an attempt to better reconstruct the vortex pair observed in the Neko-Seto Channel of the Seto Inland Sea, Japan, Park and Kaneko (2000) applied the ensemble Kalman filter (EnKF) technique of the data assimilation accompanied by the estimate of error covariance by means of the Monte Carlo method (Evensen, 1994) to analyze the first CAT data. This technique has distinct advantages in the application to strongly nonlinear current fields, and there is also no restriction in its application to the coastal seas (Madsen and Canizares, 1999). Application of the EnKF technique, as stated, was found to be the best choice to the present problem because currents in the tomography region are dominated by the strongly nonlinear tidal vortices. They found that the results obtained with the use of this method were in better agreement with the shipboard ADCP measurements (which were carried out in parallel with the CAT measurements) than those obtained by the inverse analysis of the travel-time difference data for the pairs of acoustic stations.

The simulated current fields were surprisingly improved through the implementation of the new data assimilation technique. The model result showed a tidal vortex pair composed of a western counterclockwise vortex and an eastern clockwise vortex—a result that agrees very well with observations made by aerial photographs (Takasugi et al., 1994). The tomography data are generally less accurate near the periphery of the observation region because of the decreasing number of ray paths there. Taking this limitation into account, it is justifiable to conclude that the data assimilation technique proposed by Park and Kaneko (2000) can be used as a powerful technique that is superior to the inverse analysis in analyzing the CAT data. As a result of the data assimilation, the ocean model thus reaches a level suitable for explaining the strongly nonlinear phenomena in the coastal seas.

As part of a continuing effort to improve CAT measurements in Japan, Yamaguchi et al. (2005) carried out a CAT experiment using eight source-receiver stations during March 17–20, 2003, at the Hayatomono-Seto around the Kanmon Bridge, located at the eastern part of the Kanmon Strait (Figure 7.9). The observational period included a spring tide. The area of the tomography domain was about 2 km × 2 km. The northern part of the region is characterized by a narrow trench with depths of 16–20 m, the existence of which is attributed to a strong tidal jet flushing out westward from the narrow passage where the

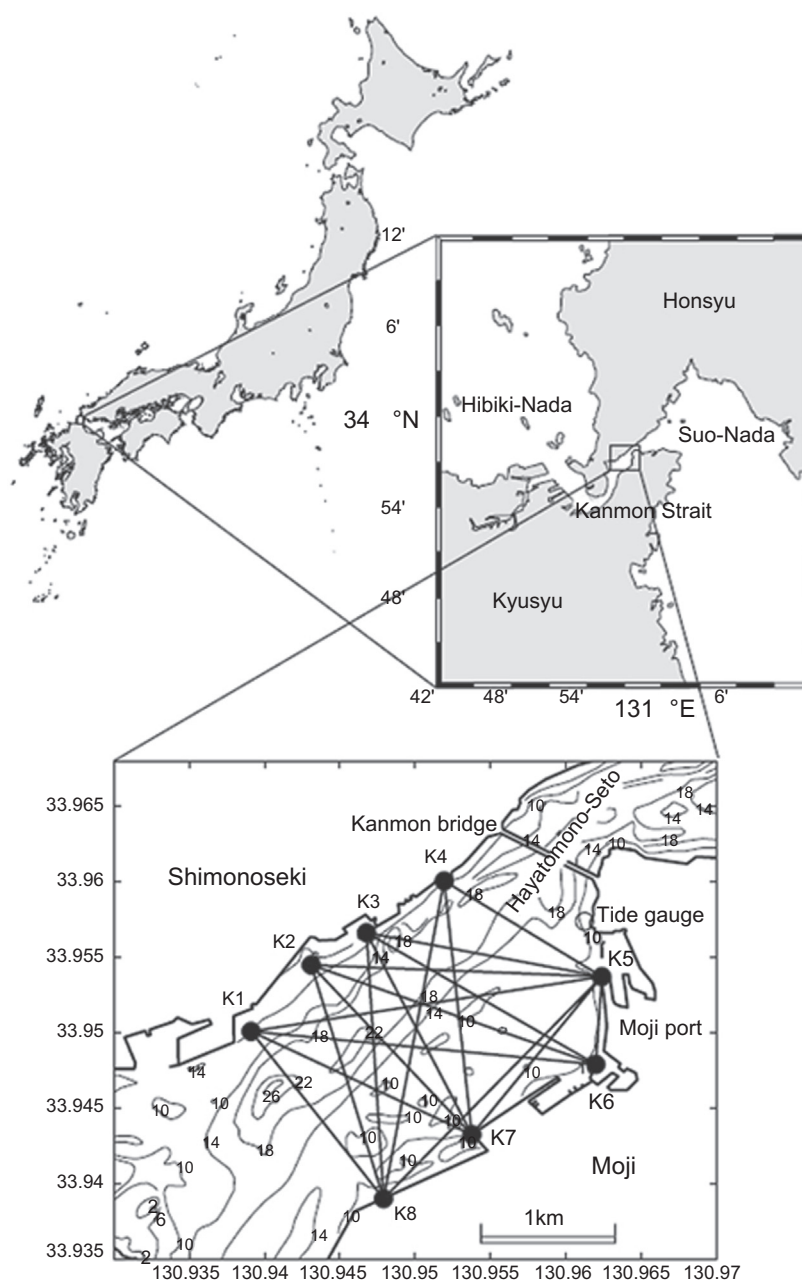


**FIGURE 7.9** Location maps of the experimental region (Hayatomo-Seto of the Kanmon Strait, Japan). The positions of the CAT stations K1-K8 and the bathymetric contours are shown in the most magnified figure with solid circles and thin solid lines, respectively. The thick solid lines connecting the CAT stations are the sound transmission lines. An interval of contour lines is 4m. (Source: Yamaguchi et al., 2005.)

Kanmon Bridge is constructed. Except for the trench, the average depth of the tomography domain is about 12 m. The seabed is mainly composed of sand.

Eight CAT systems (*K*1 to *K*8) were located at the northern and southern coasts using wharfs and piers. The strong tidal current in the strait and the safety traffic strategy of the Japan Coast Guard prohibited deployment of

the CAT system in water off wharfs and piers, even near the coast. Thus the main portions of CAT, such as the electronic housing, battery box, and GPS antenna, were placed on the ground near the edge of wharfs and piers, and only transmitters and four hydrophones were placed in subsurface water, using a steel frame in touch with their vertical walls (see Figure 7.10).

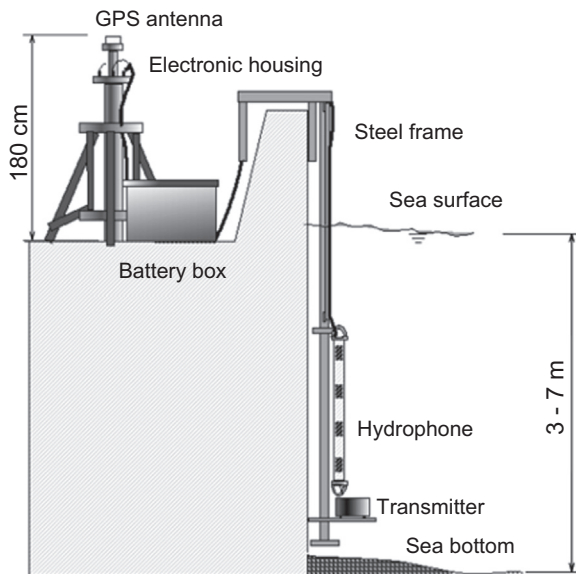


**FIGURE 7.10** Schematic diagram of the CAT system deployed at the front of wharves or piers. (Source: Yamaguchi et al., 2005.)

A pseudo-random signal, called the *10th order Gold sequence*, was transmitted every 10 minutes from the broadband transmitter (ITC2011/ITC2040) of central frequency 5.5 kHz. The 5.5-kHz carrier is modulated by the Gold sequence with a different code for each acoustic station, and one period (0.56 s) of the modulated signal is transmitted. One digit (0.54 ms) of the Gold sequence, which is the minimum unit of the Gold sequence, was set to include three waves of the carrier. The transmission signals were received by the four-hydrophone array located mainly on the opposite side of the strait. The two-way sound transmission and reception on one side of the strait were possible only between the station pairs K5–K7 and K5–K8. The received signals were preamplified, complex demodulated, cross-correlated with the Gold code, digitized by the A/D converter, and recorded into the memory. In the original schedule, the sampling frequency of the A/D converter was set to 11 kHz, i.e., two samples per wave. The relationship between the travel-time difference ( $\Delta t$ ) and the station-to-station range ( $L$ ) with the range-averaged current velocity ( $u_m$ ) as a parameter is shown in Figure 7.11. Note that the time resolution ( $t_r$ ) for multiple arrival rays in the shallow-sea sound transmission is defined by one-digit length of the Gold code (Zheng et al., 1997).

All timings of transmission, reception, and A/D conversion were synchronized by the GPS high-precision clock, which has an accuracy of about  $\pm 500$  ns. The operation of the CAT system was controlled by the internal host computer, and various parameters to specify experimental conditions were configurable at any time by connecting the external host computer with the internal one via the infrared data association.

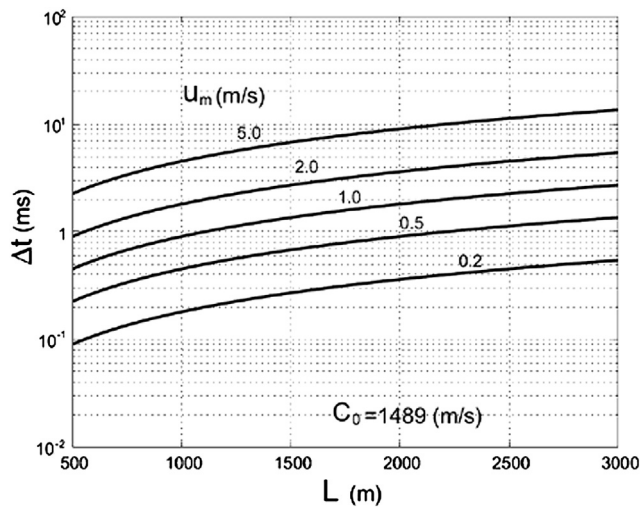


**FIGURE 7.11** Relationship between the travel-time difference ( $\Delta t$ ) and the station-to-station range ( $L$ ) with the range-averaged current velocity ( $u_m$ ) as a parameter. Here, the reference sound speed  $C_0$  is given to be 1,489 m/s from the reference values for temperature, salinity, and water depth:  $T_0 = 10.45^\circ\text{C}$ ,  $S_0 = 33.03$ , and  $D = 5$  m. (Source: Yamaguchi et al., 2005.)

The tomography data are obtained as integral values of current velocity along the ray paths. If sound speed has inhomogeneous distribution in seawater, rays draw a curve obeying Snell's law of refraction. Each eigen ray may be determined by a set of the following ordinary differential equations (Pierce, 1989; Dushaw and Colosi, 1998):

$$\begin{aligned} \frac{d \cos \theta}{dr} &= -\sin \theta \left( \frac{1}{C} \frac{\partial C}{\partial r} \tan \theta - \frac{1}{C} \frac{\partial C}{\partial z} \right) \\ &+ (3 + \tan^2 \theta) \frac{u}{C^2} \frac{\partial C}{\partial r} - \frac{1}{C} \frac{\partial u}{\partial r} - \tan \theta \frac{u}{C^2} \frac{\partial C}{\partial z} \end{aligned} \quad (7.18a)$$

$$\frac{d \sin \theta}{dr} = \cos \theta \left( \frac{1}{C} \frac{\partial C}{\partial r} \tan \theta - \frac{1}{C} \frac{\partial C}{\partial z} \right) + 3 \frac{u}{C^2} \frac{\partial C}{\partial z} - \frac{1}{C} \frac{\partial u}{\partial z} \quad (7.18b)$$

$$\frac{dz}{dr} = \tan \theta \left( 1 - \frac{u}{C \cos \theta} \right) \quad (7.18c)$$

$$\frac{dt}{dr} = \frac{1}{C \cos \theta} - \frac{u}{C^2} (2 + \tan^2 \theta) \quad (7.18d)$$

The acoustic ray paths are determined from the integral of Equation 7.18.

In the original ray-tracing method, no transmission losses of sound are taken into consideration. Yamaguchi et al. (2005) modified the original method to evaluate the acoustic intensity of transmission signals by considering the dominant transmission losses along a ray. The acoustic intensity along a ray is dissipated by transmission losses

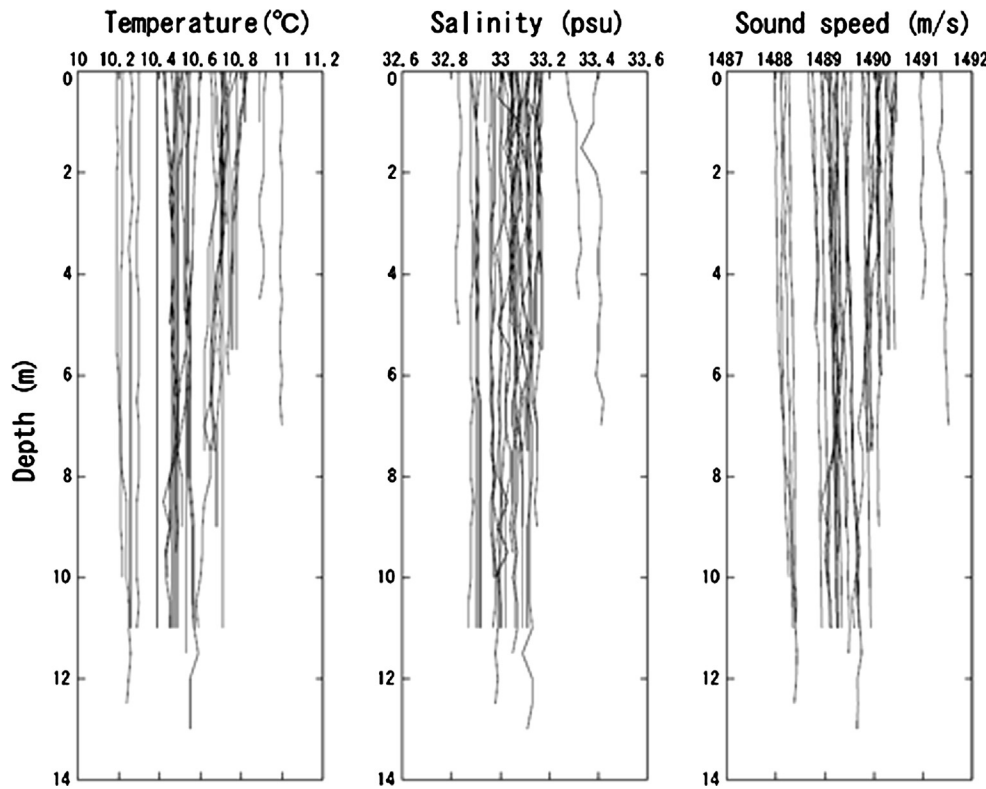


**FIGURE 7.12** Vertical profiles of temperature, salinity, and sound speed obtained at all CAT stations. (Source: Yamaguchi et al., 2005.)

due to spreading, absorption, reflection, and scattering. The sound transmission losses in shallow water may be written as:

$$TL = 10 \log r + 10^{-3} \alpha r + L_B + L_s \quad (7.19)$$

In this expression,  $r$  is the range (in meters) between the source and receiver,  $\alpha$  is the absorption coefficient (dB/km),  $L_B$  the bottom loss, and  $L_s$  the surface loss. The absorption coefficient,  $\alpha$ , may be expressed in terms of the frequency of sound ( $f$ ) as:

$$\alpha = 3.3 \times 10^{-3} + \frac{0.11f^2}{1+f} + \frac{44f^2}{4100+f^2} + 3.0 \times 10^{-4}f^2 \quad (7.20)$$

In shallow water such as the Kanmon Strait, sound waves can propagate in a duct between the sea surface and the seabed. That is why cylindrical spreading of sound is applied in the first term of Equation 7.19. The second term indicates the absorption loss, depending on the square of frequency, and according to Yamaguchi et al. (2005), it is mainly caused by the relaxation of magnesium ions in sound waves. At the third term, the bottom loss depends on the incident angle of sound wave and the seabed roughness and materials. Yamaguchi et al. (2005) used the following formula for interfaces with a random roughness (Jensen et al., 1994):

$$BL = 10 \log(\mu(\theta) \exp(-0.5\kappa^2))^{-1} \quad (7.21)$$

In this expression,  $\mu$  is the reflection coefficient and  $\kappa$  is the Rayleigh roughness parameter with the following relationship:

$$\mu = \frac{(\rho_2 C_2 / \sin\theta_2) - (\rho_1 C_1 / \sin\theta_1)}{(\rho_2 C_2 / \sin\theta_2) + (\rho_1 C_1 / \sin\theta_1)} \quad (7.22)$$

$$\kappa \equiv 2k\sigma \sin\theta_1 \quad (7.23)$$

In these equations,  $(\rho_1, C_1)$  and  $(\rho_2, C_2)$  are the (density, sound speed) pertaining to (seawater, flat seabed), respectively. Also,  $\theta_1$  and  $\theta_2$  are the grazing angle to the seabed and the refracted angle measured from the seabed, respectively. Further,  $k$  is the acoustic wave number and  $\sigma$  is the RMS roughness of the seabed. In the experiment of Yamaguchi et al. (2005), they chose  $k = 23.2$  and  $\sigma = 0.3m$  in a rough estimation.

Figure 7.12 shows the vertical profiles of temperature, salinity, and sound speed obtained by CTD measurement at the eight CAT stations, in which the sound speed was calculated by Mackenzie's formula. Water was well homogenized (i.e., no stratification) at every CAT station due to strong tidal currents. The averaged profile calculated from all the profile data was used in the ray simulation. Figure 7.13 shows the result of ray simulation obtained between the CAT

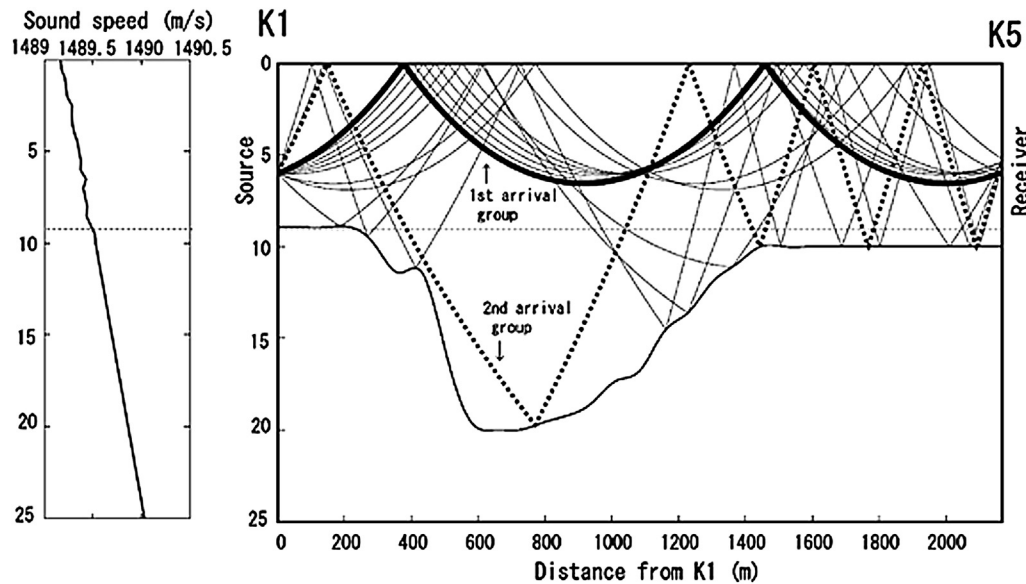


**FIGURE 7.13** Ray simulation result between CAT stations K1 and K5 determined by the ray-tracing method. Only the rays with S/N ratios greater than 10 at the receiver position are drawn. The average sound-speed profile used in the simulation is presented left of the figure. (*Source: Yamaguchi et al., 2005.*)

stations K1 and K5 as a typical example. The acoustic intensity (signal level) of received signals at the hydrophone position was evaluated by the modified ray simulation, which can consider the transmission losses along the ray.

The correlation waveforms of signals released from K1 and received at K5 are shown typically in Figure 7.14, together with the arrival signal pattern calculated by the modified ray simulation. The tiny effect of current was not considered in this ray simulation. The simulated ray arrival peaks are located inside the flattened broad peaks in the real data (Figure 7.14a), implying that the broad peaks are composed of multiarrival rays (Figure 7.14c) separated into two groups (Figure 7.14b). The travel time for the typical ray path at the first arrival group (thick solid line) passing the upper 7 m layer was determined at a time (dot) when the S/N ratio was over 10 dB at the upward-sloping front of the broad peak. A typical ray path for the second arrival group is drawn with a thick dotted line in Figure 7.14b. The 10-minute interval data for travel time were further smoothed through a one-hour running mean to reduce high-frequency variations existing in the strong current. Hourly maps of the horizontal current distributions from 6:00 to 17:00 of March 18, 2003, obtained by the inversion analysis, are shown in Figure 7.15. CAT stations with successful sound transmission are connected with solid lines. Hourly plots of the maximum current velocity and the average current velocity across the transect K2-K7 are shown in Figure 7.16.

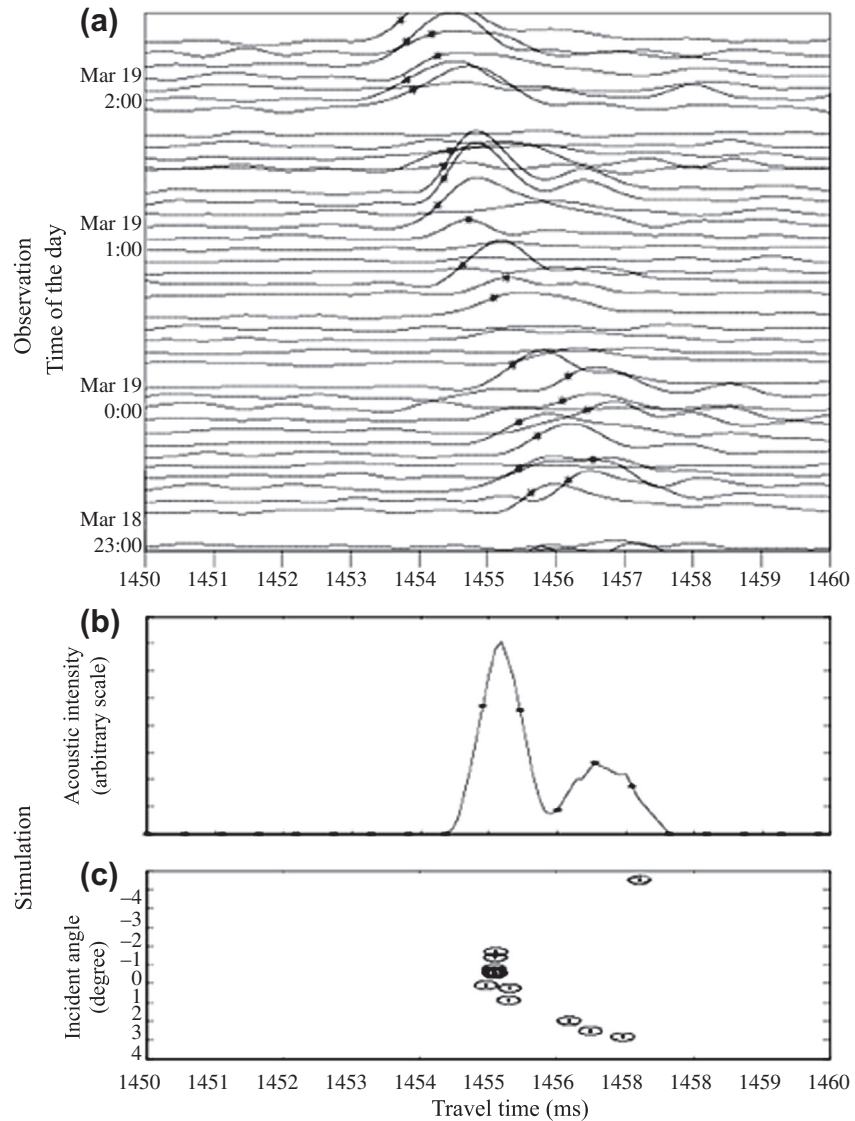
The correlation diagram between the CAT and ADP data is presented in Figure 7.17. The correlation rates for the east-west current ( $u$ ) and north-south current ( $v$ ) are 0.84 and 0.82, respectively. The RMS difference is

0.47 ms<sup>-1</sup> for  $u$  and 0.48 ms<sup>-1</sup> for  $v$ . At an overall view, the CAT velocities are considerably smaller than the ADP velocities. Yamaguchi et al. (2005) reckons that the observed difference in the measurements obtained from the two systems may have been caused by the different averaging procedure: The average along a ship track was adopted for the ADP data, whereas the CAT data were averaged through a resolution window on a horizontal plane.

The agreement between the CAT and ADP data is considered to be satisfactory regarding the maximum tidal current magnitude reaching 5 m/s and the time resolution of 0.54 ms (one-digit width) corresponding to the velocity bias of about 0.3 m/s. As for the operational system of the Kanmon Strait, the use of higher-frequency sound of about 20 kHz is considered optimal to get velocity accuracy better than 0.1 m/s. The acoustic tomographic measurements at Kanmon Strait indicate that the daily mean transport for the upper 7-m layer across the transect K2–K7 is directed eastward; Yamaguchi et al. (2005) estimated this transport to be about 1,470 m<sup>3</sup>s<sup>-1</sup> during a spring tide. The daily mean eastward transport at the spring tide is strongly supported by the three-dimensional Kanmon Strait model, which is validated with the just-mentioned CAT and ADP data. The CAT experiment conducted by Yamaguchi et al. (2005) demonstrates the ability to monitor strong tidal current structures in the Kanmon Strait.

The tidal current in the Kanmon Strait is as strong as 5 m/s at the phase of maximum tidal current. It was found that significant numerical errors are produced in the tomographic inversion. The Kanmon Strait acoustic tomography data acquired at 5-min intervals by Yamaguchi

**FIGURE 7.14** (a) Stack diagram of the correlation waveforms of signals released from K1 and received at K5 accompanied by (b) the acoustic intensity and (c) ray travel time calculated at the receiver by the modified ray simulation. (*Source: Yamaguchi et al., 2005.*)



et al. (2005) were assimilated sequentially by Lin et al. (2005) into a 2D ocean model on the basis of the EnKF scheme to image strong tidal current structures occurring in the strait. When the accurate range-averaged currents obtained for the sound transmission lines connecting eight tomography stations were used as assimilation data, the complicated vortex-imbedded currents were imaged with horizontal resolution and accuracy much better than the result of tomographic inversion. The assimilated currents were well compared to the shipboard ADCP data with a RMS difference of about 24 cm/s for both the horizontal velocity components. The assimilated volume transport across the strait also showed good agreement with the transport estimated from the range-averaged current on a pair of transmission lines crossing the strait, making a RMS difference of 3,700 m<sup>3</sup>/s. It was concluded that the

prediction of tidal current structures is useless in the Kanmon Strait with a strong forcing at the open boundaries, and instead their continuous imaging at 5-min intervals is the best policy to be taken.

The success of CAT experiments in the Japan Sea began to show its influence being permeated into the neighboring China Sea. For example, Zhu et al. (2010) successfully carried out a tomography experiment with seven acoustic stations (CAT systems) during July 12–13, 2009, in the Zhitouyang Bay near the Zhoushan Island, facing the mouth of Hangzhou Bay (China). The water depths are deeper than 40 m in the southwestern part of the bay and shallower than 20 m in the northeastern part. The maximum and minimum water depths are 91 m and 3 m, respectively, inside the tomography domain (about 11.4 km × 11.5 km). The inverse results provided continuous maps of horizontal

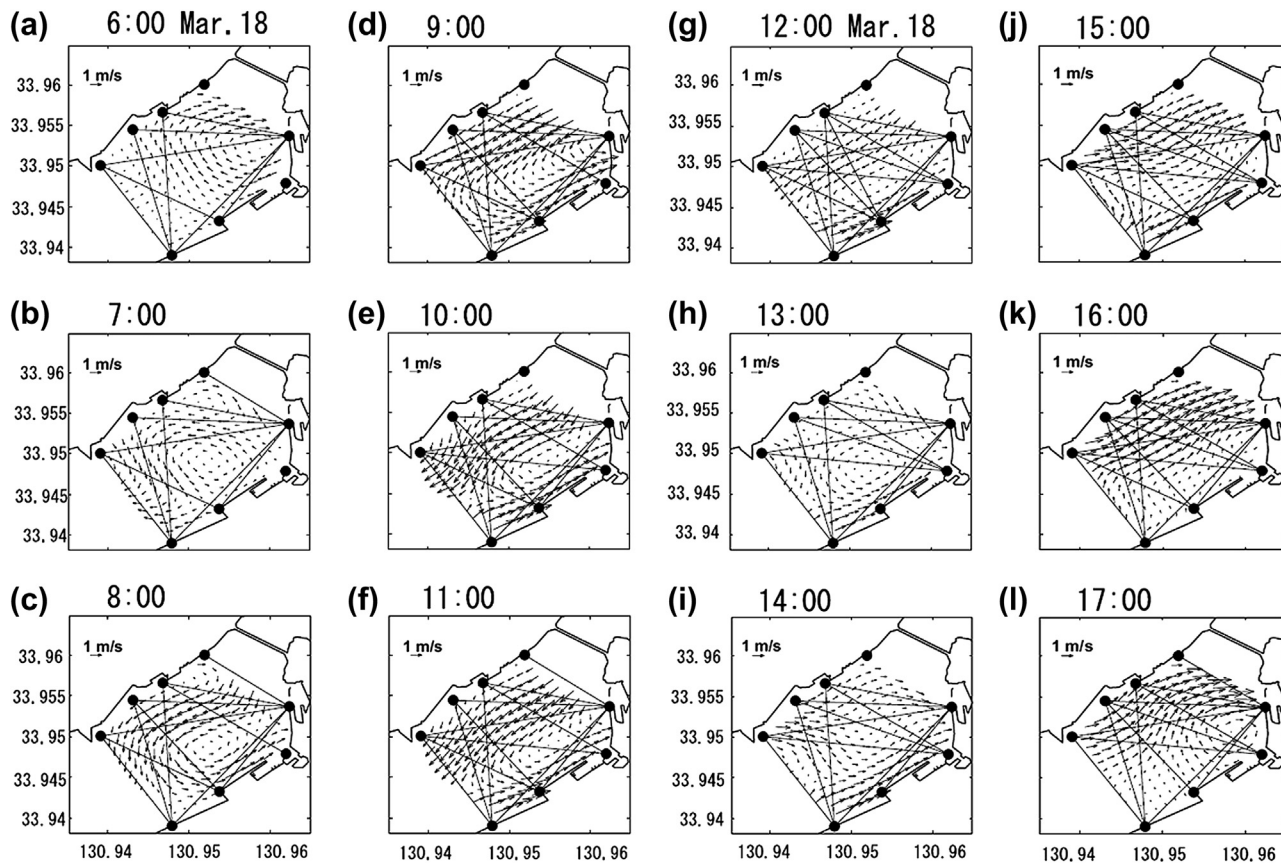


**FIGURE 7.15** Hourly maps of the horizontal current distributions during 6:00 to 17:00 of March 18, 2003, obtained by the inversion analysis. CAT stations with successful sound transmission are connected with solid lines. (*Source: Yamaguchi et al., 2005.*)

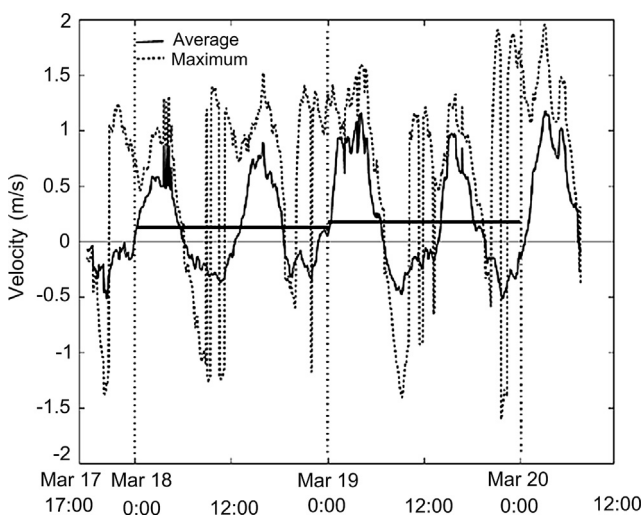
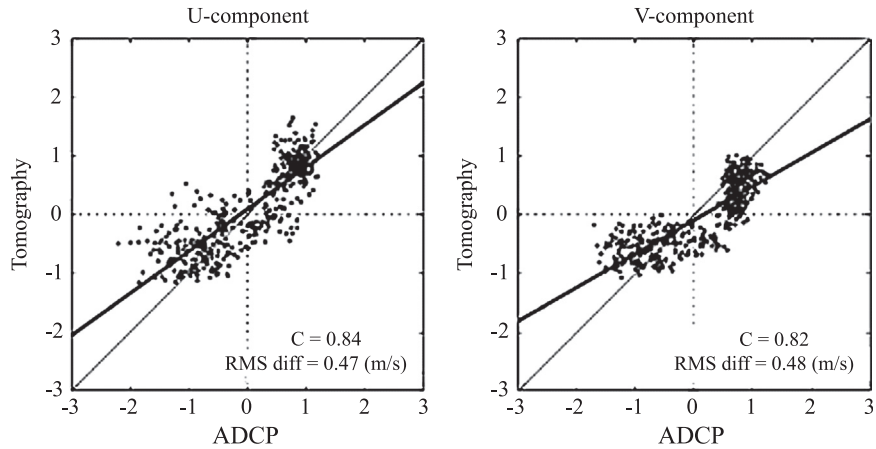


**FIGURE 7.16** Hourly plots of the maximum current velocity (thin dotted line) and the average current velocity (thin solid line) across the transect K2–K7. The daily mean velocity for March 17 and 18 is indicated with thick horizontal solid lines. (*Source: Yamaguchi et al., 2005.*)

tidal current distributions at 3-min intervals. It was found that the strong eastward tidal current, with a maximum velocity of 2.34 m/s, entered into the tomography site from the western part of the bay and separated into two branches during the ebb tide. The horizontal tidal current fields (strong eastward tidal currents with two branches during the ebb tide and the reverse currents during the flood tide) were well reconstructed by the inverse analysis of reciprocal travel-time data. The clockwise tidal vortex of size 5 km at the eastern part of the bay in the transition phase from the ebb to flood was also reconstructed. Another piece of information gained from the tomographic experiments was the absence of tidal vortices in the weak tidal currents in the transition phase from the flood to ebb while changing the current direction from westward to eastward.

The observed travel-time difference ( $\Delta t$ ) in this relatively shallow region could be well simulated by harmonic analysis, which considered eight major tidal constituents, K1, M2, M3, M4, 2MK5, M6, 3MK7, and M8. This result was found to be so useful not only for interpolating and smoothing the raw  $\Delta t$  dataset but also for predicting  $\Delta t$  values for future applications. The tomographic scheme field-tested by Zhu et al.

**FIGURE 7.17** Correlation diagrams between CAT and ADCP data. (Source: Yamaguchi et al., 2005.)



(2010) makes it possible to predict tidal currents inside the tomography domain by the inverse analysis from the known  $\Delta t$  data without relying on any tidal circulation model or data assimilation method. These results suggest that the CAT is a quite powerful instrument for continuously mapping the horizontal tidal current structures in coastal regions with heavy shipping traffic and active fishing.

## 7.5. RIVER ACOUSTIC TOMOGRAPHY

River discharge is an important hydrological quantity in terms of flood control and the management of water resources. This parameter is also important for river and coastal planning/management, control of water resources, and the like. Therefore, establishment of appropriate methods and technologies for measurement of water discharge assume great practical significance. Evidently, continuous progress of discharge measurement methods is an important issue. Conventional current measurement methods, such as ADCP (Lin, 2003), can only observe the current along a linear array. To acquire long-term data of cross-sectional average velocity and resulting river discharge, arrays of current meters should be deployed over the stream section of the river. Unfortunately, long-term measurement of river streams is often prohibited by heavy shipping traffic, especially in large rivers. As a traditional method, a water-level meter (He, 2008) is often operated to measure the discharge of nontidal rivers. However, in large tidal rivers, water level may not be a good parameter to quantify river discharge because of the nonapplicability to time-varying flows. Unfortunately, it is very difficult to measure cross-sectional mean water velocity in complex flow regimes such as tidal estuaries or during extreme hydrologic events.

Equipment that is available for continuous measurement of water discharge includes acoustic velocity meters (AVMs), horizontal acoustic Doppler current profilers (H-ADCPs), and the like (Catherine and DeRose, 2004;

Wang and Huang, 2005). The main drawback of the conventionally used methods is that often the number of velocity-sampling points in the cross-section of stream is insufficient to realistically estimate cross-sectional averaged flow velocity. Although several methods have been introduced to estimate the flow-velocity distribution (e.g., Chiu and Hsu, 2006), the results are disputable in complex flow fields such as stratified tidal flows. This calls for an innovative method and instrumentation for continuous measurement of water discharge in tidal estuaries. Taking this aspect of the problem into account, Kawanisi et al. (2009) carried out continuous water discharge measurements in a shallow tidal channel (the Ota River diversion channel), which is 120 m wide and 0.3 ~ 3 m deep, with large changes of water depth and salinity, using a new *river acoustic tomography* (RAT) system. The RAT system possesses technical advantage compared to competing techniques in terms of accurate measurement of acoustic travel time using GPS clocks and achievement of high S/N ratio due to the carrier modulation by 10<sup>th</sup> order M-sequence.

The cross-sectional averaged velocity  $v_m$  is estimated from (Kawanisi et al., 2009):

$$v_m = \frac{u_m}{\cos\theta} = \frac{1}{\cos\theta} \frac{1}{M} \sum_i^M u_{m_i} \quad (7.24)$$

In Equation 7.24,  $u_{m_i}$  is the averaged water-flow velocity along the ray path, and  $\theta$  is the angle between the ray path and the water-flow streamline. Substituting for  $u_m$  from Equation 7.12:

$$v_m = \frac{1}{\cos\theta} \frac{1}{2M} \sum_i^M \frac{C_{m_i}^2}{R_i} \Delta t_i \quad (7.25)$$

To estimate the cross-sectional average velocity  $v_m$ , the ray paths have to penetrate through all layers between bottom and water surface. If the sound speed has inhomogeneous distribution in water, the acoustic rays follow a curve

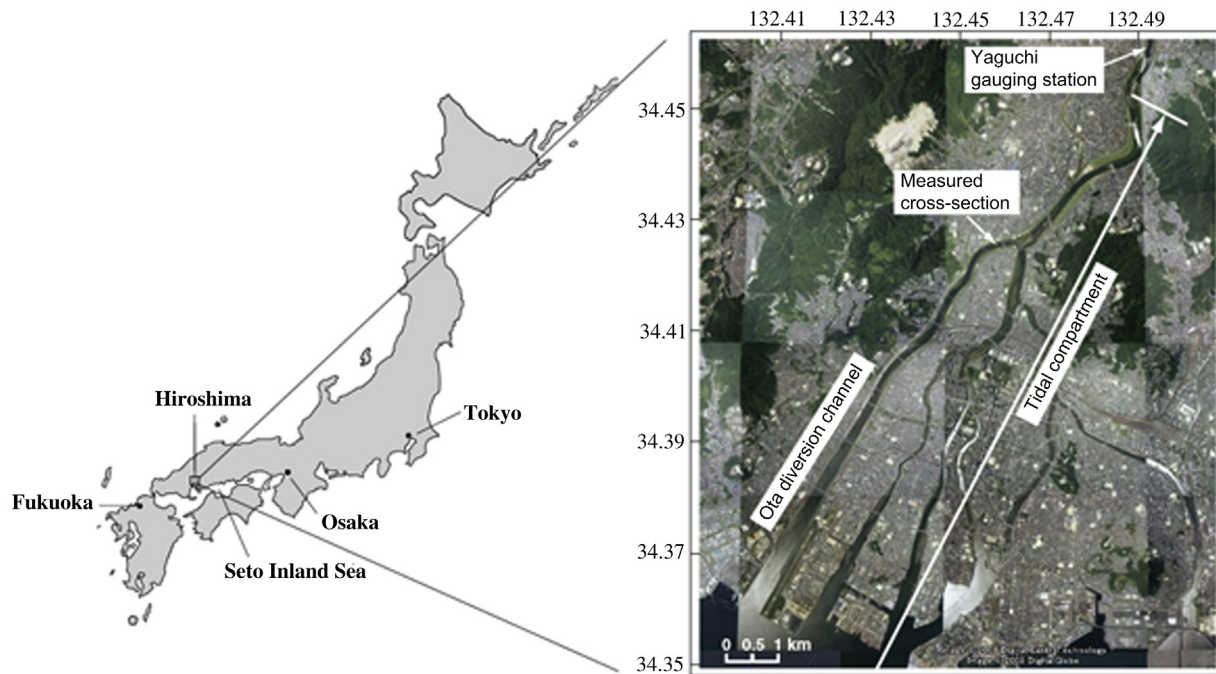


**FIGURE 7.18** RAT measurement region and experimental site in Japan. (Source: Kawanisi et al., 2009.)

obeying Snell's law of refraction. Kawanisi et al. (2009) implemented acoustic ray simulations by solving the following differential equations (Dushaw and Colosi, 1998):

$$\frac{d\varphi}{dr} = \frac{\partial c}{\partial r} \frac{1}{c} \tan\varphi - \frac{\partial c}{\partial z} \frac{1}{c} \quad (7.26a)$$

$$\frac{dz}{dr} = \tan\varphi \quad (7.26b)$$

$$\frac{dt}{dr} = \frac{\sec\varphi}{c} \quad (7.26c)$$

In these expressions,  $\varphi$  is the angle of the acoustic ray relative to the horizontal axis  $r$ ;  $z$  is the vertical coordinate; and  $t$  is the time. Kawanisi et al. (2009) estimated the in-water sound speed  $c$  using Medwin's formula (Medwin, 1975) as a function of temperature  $T$  ( $^{\circ}$ C), salinity  $S$ , and depth  $D$  (m). Water discharge can be calculated by the RAT system from the expression (Kawanisi et al., 2009):

$$Q = A(H)v_m \sin\theta = A(H)u_m \tan\theta \quad (7.27)$$

In this expression,  $A$  is the cross-sectional area in which sound paths travel (i.e., the cross-sectional area bounded between the acoustic transceivers), and  $H$  is the water level.  $A(H)$  implies that the cross-sectional area is a function of  $H$ , which undergoes temporal variability imposed by tidal height variability.

Kawanisi et al. (2009) reported a RAT experiment that was carried out during June and July 2008 at the Ota River

diversion channel. The upstream border of the tidal compartment in the Ota River estuary is about 13 km upstream, far from the mouth. The tidal range of an extreme spring tide at the mouth is about 4 m. The measurement site was located at 246 m downstream from the Gion sluice gates, as shown in Figures 7.18 and 7.19. The Ota River diversion channel at the site is 120 m wide and the water depth ranges from 0.3 m to 3 m by tide. The saltwater in this river can intrude to about 11 km upstream from the mouth.

A couple of broadband transducers were installed diagonally across the channel as shown in Figure 7.19. The

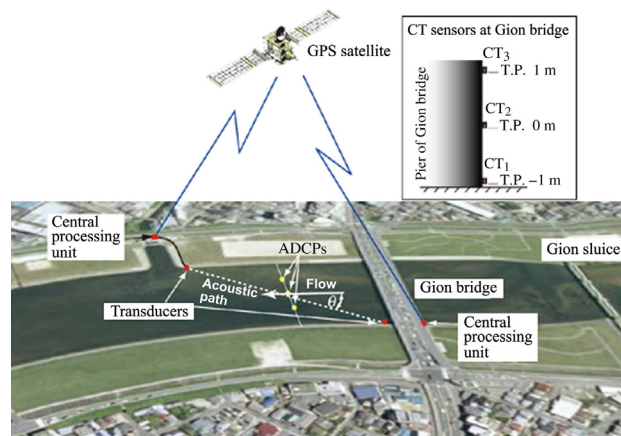


**FIGURE 7.19** Schematic of RAT measurement method in Ota River, Japan. (Source: Kawanisi et al., 2009.)

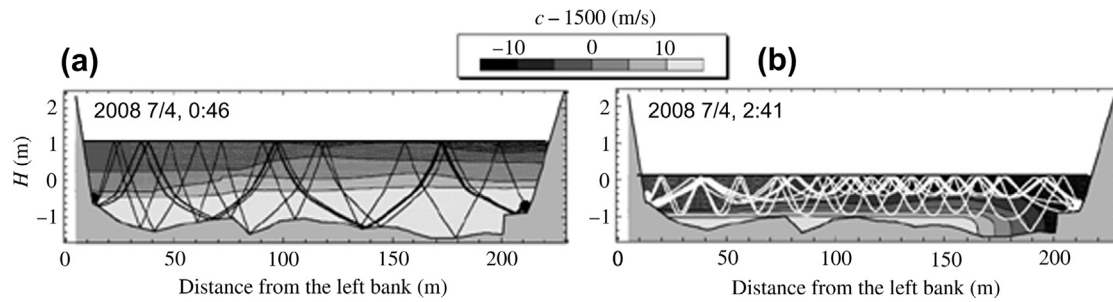


**FIGURE 7.20** Distributions of sound speed at the RAT measurement site in Ota River, Japan, and results of ray simulation. (Source: Kawanisi et al., 2009.)

central frequency of transducers was 30 kHz. The angle  $\theta$  between the acoustic ray path and the stream direction was  $30^\circ$ . The transducers were mounted at a height of 0.2 m above the river bottom. The altitudes of left and right transducers were  $-0.46$  m and  $-0.70$  m, respectively. The sound pulses of the RAT system were simultaneously transmitted from the omnidirectional transducers every minute, triggered by a GPS clock.

Three moored ADCPs were used to validate the velocity data obtained from the RAT system. These three ADCPs were arranged along the Gion Sluices in a way that each of two ADCPs were 30 m away from each other while the central ADCP location aligned with the river centerline. The distance between each ADCP and the Gion Sluice was 59.1 m.

Vertical distribution of water temperature and salinity was measured every 10 minutes by CTD sensors attached to the pier of the Gion Bridge at 40 m from the left bank. In addition, cross-sectional distributions of temperature and salinity were measured by CTD casts from the Gion Bridge. The transverse interval of the CTD casts was 20 m and crossing time was about 10 minutes.

Figure 7.20 shows distributions of the sound speed and results of the ray simulation just after HWS and just before LWS as typical examples. The tiny effect of current is not considered in the ray simulation. The sound speed was calculated from projected data of the CTD cast from the Gion Bridge. The salinity increases with depth, and as a result of this distribution, sound speed ranged from 1,515 m/s in deeper layers to 1,485 m/s near the surface.

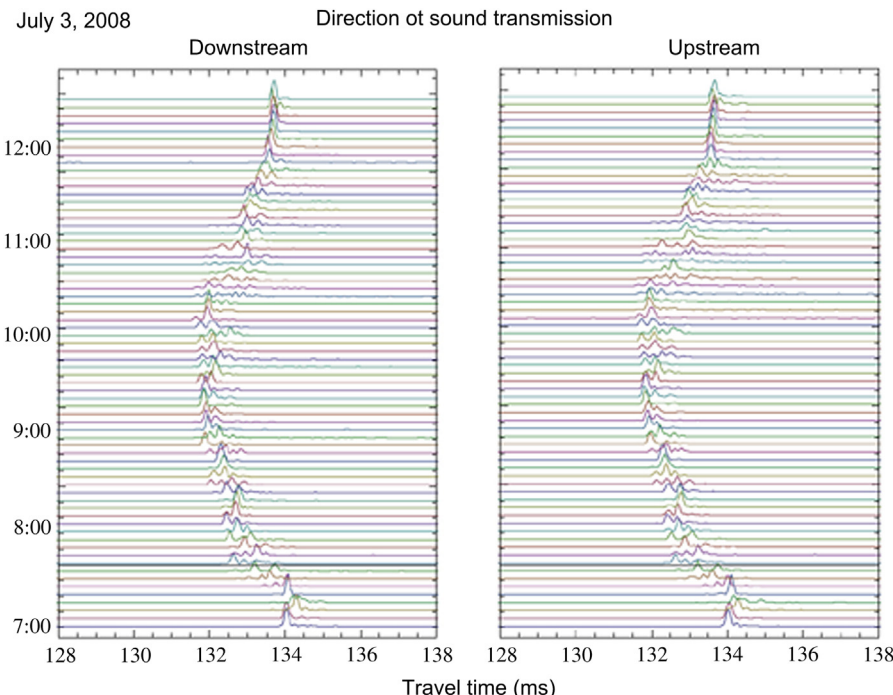


**FIGURE 7.21** Stack diagrams of correlation waveforms of 10<sup>th</sup> order M-sequence modulated acoustic transmissions from upstream and downstream transducers at the RAT measurement site in Ota River, Japan. (Source: Kawanisi et al., 2009.)

Most of the time, the sound paths cover the cross-section, as shown in Figure 7.20a. At times a near-bed-established salt wedge caused the sound paths to be reflected; consequently, a part of sound paths were not able to penetrate into the lower layers; a typical condition under strong stratification is depicted in Figure 7.20b. In this case, the cross-sectional averaged velocity is somewhat overestimated by the RAT system. For this reason, the cross-sectional averaged water-flow velocity had to be modified using velocity distribution of two-layer flow when there was a salt wedge under the transducer.

The cross-correlation waveforms of signals transmitted from the upstream and downstream transducers (plotted every 5 min) are shown typically in Figure 7.21. The fact that the cross-correlations obtained from both sides are of similar form suggests that the two-way path geometry is reciprocal. The broad peaks are composed of multiarrival rays. It seems that the single peak is also composed of multiarrival rays because the experimental site is shallow. The mean arrival time changes because of salinity change. Sometimes there were no clear peaks. In the study reported by Kawanisi et al. (2009), the two-way travel-time difference was calculated when the S/N ratio was over 14.

Figure 7.22 shows temporal variations of the cross-sectional averaged velocity,  $v_m$ , and the water level,  $H$ . The thick red line denotes the cross-sectional averaged velocity deduced from three moored ADCPs. The broken line denotes the water level. Because of the strong nonuniformity of flow at the observation site, data from just three ADCPs were unlikely to have well represented the cross-sectional averaged velocity. Despite this lacuna, the difference between water-flow velocities acquired by the RAT system and the ADCP is small. The observed comparison implies that the cross-sectional averaged velocity obtained from the RAT system fulfills an

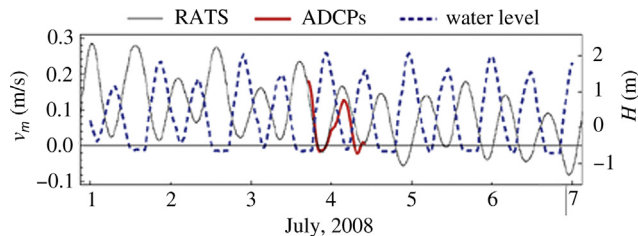


**FIGURE 7.22** Comparison of cross-sectional averaged water-flow velocity between RATS and ADCPs at the RAT measurement site in Ota River, Japan. (Source: Kawanisi et al., 2009.)

acceptable compliance with the results derived from an array of ADCPs.

Temporal variations of water levels at Yaguchi and Gion and the flow discharge for 44 days are illustrated in Figure 7.23. It was found that the water discharge values modified using velocity distribution of two-layer flow were, on an average, ~10 percent smaller than those without correction for the observation period. It is interesting to note that the pattern of the trend of discharge, denoted by a thick line, closely resembles that of the change of water level at the Yaguchi gauging station. These observations indicate that employing RAT system is a promising method for continuous measurement of water discharge in rivers and estuaries.

Although the reciprocal sound transmission method has been employed as an innovative technology to continuously measure the cross-sectional average velocities in a tidal channel in Japan (Kawanisi et al., 2009), no such experiments were attempted to measure the variation of discharge in tidal rivers in China. However, Zhang et al. (2010) reported such an experiment, which was performed in the Qiantang River as the first application in China.

Zhang et al. (2010) carried out reciprocal sound transmission experiments for current measurement in the

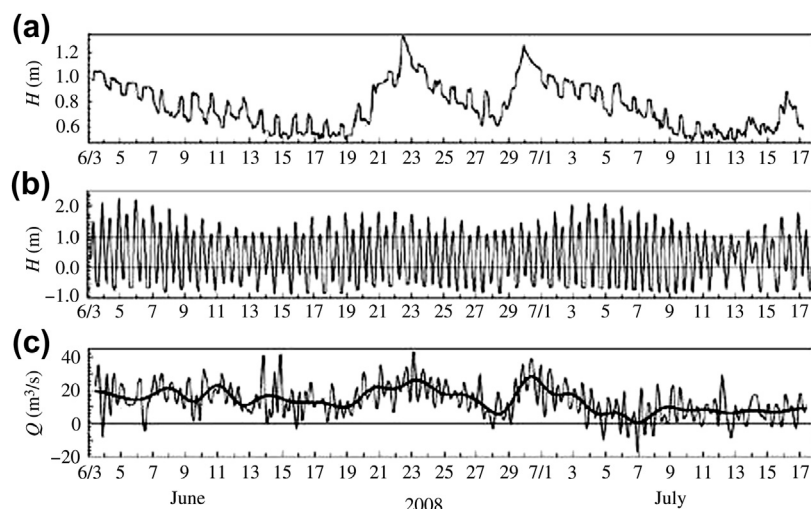


**FIGURE 7.23** Temporal variations of water levels at (a) Yaguchi and (b) Gion at the RAT measurement site in Ota River, Japan, and (c) water discharge for 44 days. (Source: Kawanisi et al., 2009.)

upstream region of the Qiantang River, about 90 km from the mouth of Hangzhou Bay from April to December 2009. This estuary is notorious for the occasional occurrence of the dreaded tidal bores. Two systems were set up at stations east and west with a distance of 3,050 m across the Qiantang River. The transducer (a Neptune T170) was suspended down to 3 m depth through a rope from the wharf; the system components such as electronic housing, battery, and GPS antenna were placed on the wharf. The 5-kHz sound signal, modulated by one period (0.64 s) of the pseudo-random signal, called the 10th order M-sequence, was transmitted every 3 min from the broadband transducer.

Reciprocal sound transmissions were successfully performed along the sound transmission line. The travel time changed in the range 2.033–2.103 s during the whole experimental period, conforming to the expected travel time of about 2.061 s between the two stations (3,050 m / 1,480 m/s = 2.061 s). The reciprocal travel time decreased suddenly at the arrival of tidal bores. Also, travel time from west to east is larger than that from east to west. The changes in travel time during the arrivals of tidal bores are caused by the sound-speed changes due to the downstream increase of water temperature along the Qiantang River (because salinity is nearly zero).

The time plots of the path-averaged alongstream water-current flow velocity were estimated using the travel-time difference data. The tomographically measured and ship-board ADP velocities were in good agreement, producing a root-mean-square difference (RMSD) of 0.03 m/s. The tomographically measured water-current flow velocity made a dramatic change during the arrival of tidal bores. Before their arrival, freshwater flowed eastward from upstream to downstream with velocities ranging from 0.25 m/s to 0.82 m/s. The eastward freshwater flow became weak and then changed its directions from eastward to westward within a short period of about 20 minutes when the tidal surges arrived at the experiment site. This westward flow reached maximum velocities ranging from -0.11 m/s to -1.18 m/s, then kept its direction and magnitude for about 100 minutes constant. This westward flow was gradually replaced by the eastward flow, and this “drama” finished in about 5 hours and 20 minutes after the arrival of the tidal bores. This “drama” occurred twice one lunar day in a synchronized timing with the semidiurnal tide in Hangzhou Bay.

The acoustic travel-time differences  $\Delta\tau$  data have been found to be well correlated with the ADP data ( $Q_{ADP}$ ), with a linear relation. The correlation coefficient is 0.99, and the RMSD from the regression line is 241 m<sup>3</sup>/s. It was found that the empirical formula that connects tomographically obtained river discharge ( $Q_{TOMO}$ ) and  $\Delta\tau$  may be expressed by (Zhang et al., 2010):

$$Q_{TOMO} = -2400 \times 10^3 \Delta\tau + 179 \quad (7.28)$$

Zhang et al. (2010) estimated the river discharge during the whole experimental period in a time series through this empirical formula. It is seen that  $Q_{TOMO}$  has a quite good agreement with  $Q_{ADP}$ . The variations of the river discharge were very similar to those of the velocity. During the arrival of tidal bores,  $Q_{TOMO}$  changed not only in its values but also in its directions, meaning that the river discharge changed from eastward to westward. The eastward freshwater discharge reached a maximum value of 5,096 m<sup>3</sup>/s during 0:00–6:30 of August 13, 2009, when a rainstorm attacked the upstream region of the Qiantang River just before the experiment. On the other hand, the maximum westward discharge of -7,626 m<sup>3</sup>/s (from downstream to upstream) occurred in the spring tide during 2:0–3:40 h of September 19, 2009, when the tidal bores became the strongest in all the experimental periods. The mean of  $Q_{TOMO}$  for the whole experimental period was 1,246 m<sup>3</sup>/s and equivalent to the averaged freshwater discharge of the Qiantang River.

## 7.6. ACOUSTIC TOMOGRAPHIC MEASUREMENTS OF VORTICITY

The concepts of vorticity and especially its conservation have played a central role in furthering our understanding of the meso- and large-scale oceanic and atmospheric circulations (Rossby, 1975; Conzemius and Montgomery, 2009). Through Gauss's theorem, the tendency of circulation for any enclosed area fixed in space can be written in terms of the line integral of the flux component normal to the boundary of the area. Circulation in an ocean basin is often associated with vorticity. Because solid Earth spins, a water mass that resides on it will suffer an additional vorticity associated with the spinning Earth. Thus, the vorticity measured by an observer on Earth is not absolute vorticity but is *relative vorticity*. Estimates of relative vorticity are necessary to determine the long-term balance of energy and momentum in an ocean basin. Muller et al. (1986) pointed out the importance of the vorticity mode of motion that must coexist with internal gravity waves at small scales. Conventional methods of measuring currents do not allow for an accurate calculation of the vertical component of vorticity on geostrophic time scales. Because relative vorticity and horizontal divergence are difficult to measure using conventional instruments, the vortical mode of motion has traditionally been ignored. Muller et al. (1988) made an attempt to measure potential vorticity at small scales in the ocean from measurements at three discrete locations using a triangular array of current meters. However, such discrete measurements can give rise to significant sampling errors because the measurements do not represent a continuous line integral (i.e., path-averaged measurement) along the sides of the triangle.

As we have already noted, reciprocal acoustic transmission methods have proved to be successful in several

experiments, and this provides optimism for the feasibility of ocean basin-wide measurements. This technique has indeed been found to be useful for estimation of relative vorticity. In fact, the most exciting application of reciprocal transmissions is considered to be the measurement of relative vorticity. This concept of determining the relative vorticity of oceanic motion in a realistic manner (i.e., from continuous path-averaged measurements) was originally suggested by Rossby (1975), although its practical implementation came much later. According to this concept, acoustic transmissions in opposite directions around a closed loop give circulation directly. This quantity, on basin scale, is quite difficult to measure using traditional approaches. In addition, its unprecedented sensitivity allows detection of phenomena not observable with traditional sensors.

Even in the absence of appropriate technologies, Thomas Rossby of Yale University's Department of Geology and Geophysics was optimistic that as more sophisticated studies of oceanic motion were mounted, increasing stress would be laid on our ability to reveal the higher-order vorticity dynamics. Accordingly, he proposed a new approach to this measurement problem, which is based on an acoustical method for determining the circulation around a closed path (Rossby, 1975). Once the circulation around a closed path is known, Stokes' theorem can be applied to obtain the average vorticity of the "enclosed" fluid. The central element of Rossby's scheme is the notion that the line integral of fluid velocity along a ray between two points is proportional to the difference in travel time of two acoustic signals, transmitted in opposite directions. (This concept has already been elaborated in this book under reciprocal acoustic method of ocean-current measurement.) If  $v$  is the velocity vector in a flow field in the direction of the flow stream, and  $s$  is a unit vector along the acoustic propagation path (which can be oriented in any direction relative to  $v$ ), the line integral of fluid motion around an  $N$ -cornered polygon (i.e., fluid circulation around the polygon) becomes  $\oint v \cdot ds$ . Stokes' theorem tells us that this fluid circulation is equivalent to the surface integral of the normal component of vorticity, but this is the average vorticity,  $\xi$ , times the area,  $A$ , encompassed by the closed loop. That is, fluid circulation around the polygon, by virtue of Stokes' theorem, is equivalent to the areal-average relative vorticity of the enclosed fluid. In mathematical terms,

$$\oint v \cdot ds = \xi \times A \quad (7.29)$$

Thus, the average vorticity is given by:

$$\xi = \frac{1}{A} \oint v \cdot ds \quad (7.30)$$

Rossby (1975) has called attention to the fact that for each side of the polygon we also have a line-averaged

current meter (equivalent to reciprocal tomographic current measurement). He suggested that if the  $N$ -cornered polygons are placed horizontally in the ocean so that only the vertical vorticity is sensed, it would be possible to determine a numerical relationship between  $\xi$  and the travel-time difference around the loop. While conceptualizing the applicability of reciprocal acoustic transmission method for estimation of vorticity, Rossby was optimistic that although the acoustic travel-time difference is very small, it would be possible with very narrow band-pass filters or phase-lock techniques to achieve the desired timing resolution (of the order of  $\mu s$ ) using a CW frequency of, say, 10 kHz.

As pointed out under the preceding discussion, estimation of relative vorticity of fluid motion in an ocean basin requires measurement of path-averaged fluid velocity around a closed loop (Figure 7.24). This, in the reciprocal acoustic transmission method, is equivalent to the measurement of travel-time differences of acoustic propagation along this closed loop. From the theory of ATT current meters (see Section 9.2), the travel-time difference  $\Delta t_{ij}$  along an acoustic ray path of range  $l_{ij}$  joining points  $P_i$  and  $P_j$  is given by:

$$\Delta t_{ij} = \frac{(2v_{ij} \times l_{ij})}{(c_{ij})^2} \quad (7.31)$$

where  $c_{ij}$  and  $v_{ij}$  are the path-averaged sound speed in seawater at rest and fluid velocity, respectively, along the ray path joining  $P_i$  with  $P_j$ . Thus,

$$v_{ij} = \frac{\Delta t_{ij} \times (c_{ij})^2}{2l_{ij}} \quad (7.32)$$

The line integral of the fluid motion between points  $P_i$  and  $P_j$  can, under the assumption that the flow is momentarily steady, be written as:

$$\int_{P_i}^{P_j} v \cdot ds = v_{ij} \times l_{ij} = \frac{\Delta t_{ij} \times (c_{ij})^2}{2} \quad (7.33)$$

where  $v$  is the velocity vector and  $s$  is a unit vector along the acoustic propagation path. Estimation of vorticity, based on

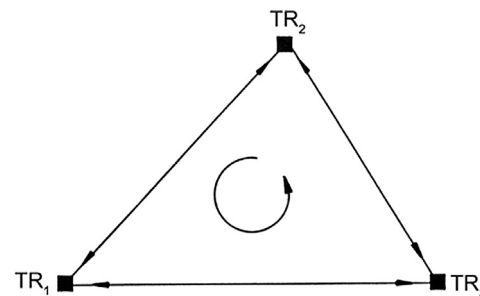


**FIGURE 7.24** Arrangement of acoustic transceivers  $TR_1$ ,  $TR_2$ , and  $TR_3$  (minimum configuration) for measurement of vorticity.

the method proposed by Rossby (1975), requires estimation of the line integral of fluid motion around a closed loop. Because a minimum of three lines are required to form a closed loop, a minimum configuration of instrumentation required for estimation of relative vorticity is a set of acoustic transceivers placed on the vertices of a triangle (see Figure 7.24). Thus, the line integral of fluid motion around a triangle  $P_1P_2P_3$  becomes:

$$\oint v.ds = (v_{12} \times l_{12}) + (v_{23} \times l_{23}) + (v_{31} \times l_{31}) = \frac{[\Delta t_{12} \times (c_{12})^2] + [\Delta t_{23} \times (c_{23})^2] + [\Delta t_{31} \times (c_{31})^2]}{2} \quad (7.34)$$

Let us make the assumption that the triangle lies on a horizontal plane. Equation 7.30 gets modified as:

$$\xi = \frac{[\Delta t_{12} \times (c_{12})^2] + [\Delta t_{23} \times (c_{23})^2] + [\Delta t_{31} \times (c_{31})^2]}{2A} \quad (7.35)$$

Assuming that  $c_{12}$ ,  $c_{23}$ , and  $c_{31}$  are nearly the same and equal to  $c$ , we get:

$$\xi = \left( \frac{c^2}{2A} \right) (\Delta t_{12} + \Delta t_{23} + \Delta t_{31}) \quad (7.36)$$

Taking into account a situation in which adequate numbers of acoustic transceivers are configured on an isosceles triangle or square of 3-km/side, placed horizontally in the deep ocean, Rossby discussed possible error budgets in the measurement of acoustic travel-time difference. According to him, although the assumption that  $c$  and  $v$  are temporarily steady is not strictly valid, if the time difference is based on simultaneously transmitted signals, as it certainly should be, then it is only a variability in the timeframe between transmit and receive that can affect the measurement (~2 seconds for a 3-km path). Variations in the water-current flow speed on this time scale will be negligible. The local speed of sound is especially stable in deep waters and for a given pressure will depend mostly on local water-temperature variations, which are of order 3–10 centidegrees. That is equivalent to changes in the sound speed of 15–50 cm/s. Such variations result from the advection of water masses, which are large compared to the polygon mentioned earlier.

The temporal variance in temperature on a “seconds time scale” is one of milli-degrees or less. The effect of this on the speed of sound is equivalent to less than 1 cm/s, and when this is also line averaged, it can be confidently stated that the path-averaged sound speed in deep water should have quite negligible variability within the 2-s timeframe (for a 3-km path). Spatial variations in the speed of sound due to temperature and salinity are

by themselves unimportant because the quantity  $\Delta t$  is a differential measurement along the same path. On the strength of these considerations and rapid advances achieved on the technology front, Menemenlis and Farmer (1992) employed this concept to measure path-averaged horizontal current and relative vorticity of water mass in the sub-ice boundary layer of the eastern Arctic.

## 7.7. HORIZONTALLY INTEGRATED CURRENT MEASUREMENTS USING SPACE-TIME ACOUSTIC SCINTILLATION ANALYSIS TECHNIQUE

An alternative acoustic method developed to measure coastal water-current flows is the *acoustic scintillation method*. The acoustic scintillation technique of flow measurement is similar in principle to the well-known tracer technique wherein a dye, a chemical, or a radioactive isotope is injected into the flowing fluid, and its transportation over a known distance is timed to estimate the flow velocity, using the definition of velocity (i.e., distance traveled in unit time). The essential difference between the tracer method and the acoustic scintillation method is that whereas a foreign substance is injected into the flow field in the tracer method, the “tracer” in the acoustic scintillation method is merely some acoustically detectable random fluctuations already existing naturally in the flow field.

The random fluctuations can take many forms, such as velocity turbulence, presence of a second phase, and temperature fluctuations. Internal waves, layering, and turbulence create inhomogeneities of sound speed in the ocean, and these inhomogeneities induce fluctuations in the ocean acoustic transmission. Through both refractive and diffractive effects, sound waves from a point source are perturbed from the simple spherical or plane-wave geometry into more complicated phase fronts (Duda and Flatté, 1988). A wave propagating through a random medium, such as a turbulent flow field, undergoes distortions in its amplitude and phase. Initially, only the phase of the wave is distorted as it propagates through the turbulent medium. These phase distortions or wrinkles in the wave front redirect the wave’s energy, eventually producing both amplitude and phase distortions and, finally, intensity fluctuations (i.e., scintillation) due to interference across some distant receiving plane (Clifford and Farmer, 1983). This results in a complicated diffraction pattern, similar in

nature to the stellar scintillations (twinkling of stars) as observed near the focal plane of an astronomical telescope. In analogy, a similar pattern at the receiver of an acoustic transducer is known as *acoustic scintillation*. The pattern of irregular intensity (the scintillation pattern) in a receiving plane, perpendicular to the acoustic propagation axis, evolves with time. The evolution of the scintillation pattern occurs because of advection and/or decay of the density fluctuations or eddies that produce the wave perturbation. If the transit time of the scintillation pattern across the detectors is short compared to the eddy lifetimes, it is possible to derive quite accurate estimates of the intervening transverse flow from a statistical analysis of the scintillation pattern.

Scintillation techniques have long been employed to elucidate the fine scale structure and motion of the turbulent media. The acoustic scintillation analysis technique is, in fact, a spin-off from the applied optics wherein the properties of the intervening medium such as ionospheric, solar, and atmospheric winds were determined from an analysis of turbulence-induced stellar scintillations. Because of the unique spatial distribution of medium irregularities for each of these applications (i.e., concentrated at one position along the path or uniformly distributed), different techniques have been devised to estimate flow information. However, in acoustic scintillation analysis only three methods have so far been applied to estimate oceanic water current flows.

Acoustic scintillation technique has successfully been used for measurement of water flows in straits and channels. The minimum configuration of a flow-measuring device that employs this technique consists of a single acoustic transmitter and two acoustic receivers located in such a way that the acoustic transmission path is transverse to the flow direction (see Figure 7.25). The separation between the transmitter and the receiver ranges from a few meters to a few km. The two acoustic receivers are placed at a known distance apart in the flow field so that the receiving planes of these two hydrophones are normal to the acoustic path. The scintillation pattern at the receiver plane drifts with the flow. Upon reception, the acoustic signal from one receiver is compared with that from the other receiver to find the time lag,  $T$ , at which the scintillation patterns at the two receivers have maximum similarity or a best fit in waveform (i.e., *autocorrelation*). It is well known that autocorrelation is a mathematical representation of the degree of similarity between a given time series and a lagged version of itself over successive time intervals. It is the same as calculating the correlation between two different time series, except that the same time series is used twice (i.e., once in its original form and once lagged one or more time periods). The term can also be referred to as *lagged correlation* or *serial correlation*. From the estimated time lag,  $T$ , and the known receiver separation, the flow velocity is computed.

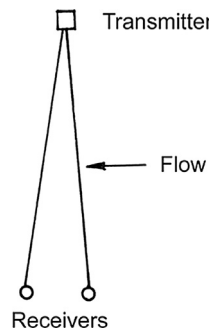


**FIGURE 7.25** Sketch of minimum configuration of an acoustic scintillation device, consisting of a single acoustic transmitter and two acoustic receivers located in such a way that the acoustic transmission path is transverse to the flow.

Flow measurement using scintillation analysis technique is based on Taylor's frozen-flow hypothesis, according to which the fluctuations in the refractive index at any point result solely from the advection of a frozen refractive index field past that point by a mean flow. This hypothesis is reasonably well satisfied by atmospheric and oceanic turbulence over short distances, but it is violated by internal waves. This is the reason that the method has not been used for measurement of flows in the open ocean where internal waves may be present. However, in straits and tidal channels, the flow is mainly driven by tide, and acoustic scintillation arises only from turbulence. In these environments Taylor's hypothesis is well satisfied and the acoustic scintillation technique can be applied for measurement of water-current flows. As the refractive index irregularities are advected *across* the acoustic propagation path, the structure in the scintillation pattern drifts across the receiving plane with a speed proportional to the flow speed if weak scattering restriction is satisfied. The value of the proportionality constant depends on the type of incident wave. For example, the pattern drift-velocity  $V_p$  for an incident spherical wave is given by  $2V_t$ , where  $V_t$  is the transverse flow velocity. The factor of 2 arises because of the diverging nature of the spherical wave field and the sensitivity of the measurement to refractive eddies at mid-path (Clifford et al., 1990). For an incident plane wave, the pattern drift velocity  $V_p$  is equal to  $V_t$ .

It has been noted that the acoustic scintillation analysis technique is applicable for flow measurement if weak scattering restriction is satisfied. Over short ranges, characterized well by a single transmission path from a source to any receiver, the wave front may be subjected to effects that are weak enough that the variation of signal amplitude in a plane transverse to the transmission path is a small fraction of the average amplitude. This is the weak scattering or unsaturated regime. Weak scattering theory has been shown to accurately describe wave transmission when the normalized variance of intensity (sometimes called the

*scintillation index*) is less than 1. For centimeter acoustic wavelength, the acoustic path length in a flow field is limited to a few km.

Two techniques that are generally used in the scintillation analysis method of flow measurements are based on peak delay and slope of covariance at zero lag. Clifford and Farmer (1983), who originally used acoustic scintillation analysis for ocean-flow measurement, employed the latter technique. In this method, a time-lagged covariance function ( $C$ ) at displacement ( $d$ ) is constructed to study the spatio-temporal variation of the scintillation patterns at the two receivers. The slope at zero time lag of the normalized covariance is proportional to the path-weighted average of the transverse flow ( $u$ ) and is given by (Clifford and Farmer, 1983):

$$m_N = \frac{1}{L} \int_0^L W_y U_y dy \quad (7.37)$$

where  $y$  is the constant plane, the refractive index fluctuations along which have given rise to the scintillation drift;  $L$  is the acoustic path length; and  $W_y$  is a weighting function. In general,  $U$  can be expressed as  $U = R \times m_N$ , where  $R$  is a calibration factor in meters.  $R$  takes different values for different turbulence spectral power laws and spacing  $B = \left(\frac{d}{R_f}\right)$ , where  $R_f$  is the Fresnel radius given by the square root of the product of the acoustic wavelength with the path length. Values of the calibration factor for different values of  $B$  and spectral power laws are given in Clifford and Farmer (1983).

In the first experiment conducted by Clifford and Farmer (1983) to test the validity of the scintillation technique for ocean-flow measurement, the acoustic transducers were mounted on two masts, which were rigidly mounted on the leading edge of a research barge that could be towed at various speed steps (see Figure 7.26). The transducers were maintained at a depth of 2.1 m below the water surface. The transmitter-receiver separation was 12.4 m. The separation of the two receiving hydrophones, oriented along a plane perpendicular to the acoustic transmission path, was set at 15.7 cm, which was approximately one-half of a Fresnel radius for the given experimental setup.

The experiment was conducted in Saanich Inlet in 1982. Both the projector ( $P$ ) and the receiving hydrophones ( $R$ ) consisted of single hexagonal elements of 6 cm diameter. The projector was driven at approximately 214 kHz with 5 cm pulses once every 100 ms. For a transmitter-receiver separation of 12.4 m, the receiving hydrophones detected only the direct pulse, without contamination by multipath propagation. The signals received at the hydrophones were amplified, detected with an rms-to-DC converter, filtered, digitized, and recorded. When the flow was zero, the signals received at both the hydrophones displayed a low-

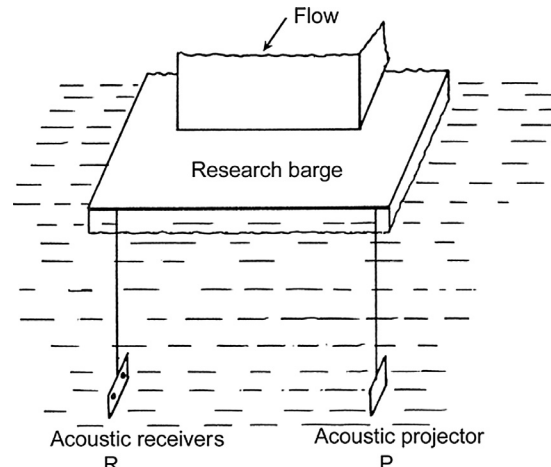


**FIGURE 7.26** A sketch of the initial experimental arrangement used to test the practicability of acoustic scintillation technique of flow measurement. (Source: Modified from Clifford and Farmer, 1983.)

frequency fluctuation associated with slowly moving and changing patterns in the refractive index along the acoustic path. With increase in flow, the signal frequency greatly increased, as anticipated on theoretical grounds.

Data analysis begins with breaking the edited time series of data received at the two hydrophones into 1-min segments, followed by log normalization and high-pass filtering. For each segment, the cross-covariance is calculated, together with the first central difference estimate of the cross-covariance slope at zero lag. Three examples of cross-covariance functions, corresponding to zero flow and flows in two opposite directions, are shown in Figure 7.27. It can be seen that the peak of the normalized covariance corresponding to zero flow lies on the zero-lag axis, whereas the peaks corresponding to nonzero flows get shifted with reference to this axis. The position of the peak also gives an indication of the flow direction.

The amount of the shift is a measure of the magnitude of the flow normal to the acoustic path. The magnitude and

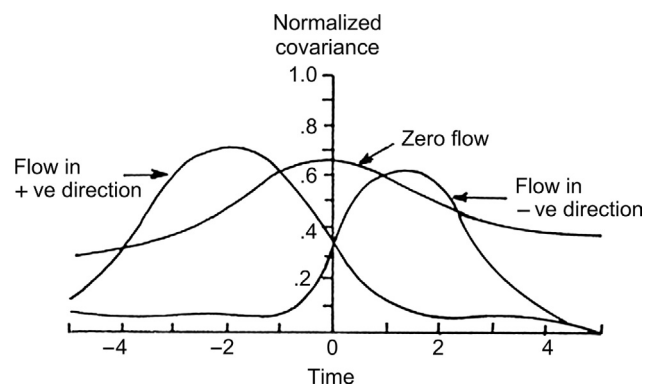


**FIGURE 7.27** Cross-covariance as a function of lag for still water and flows in opposite directions. One unit on the abscissa is 0.1-s time lag. (Source: Modified from Clifford and Farmer, 1983.)

sign of the slope of the normalized covariance at zero lag can also be used for estimation of the magnitude and direction of the flow perpendicular to the acoustic path. Initial experiments have indicated that the time series of path-averaged flow transverse to the acoustic propagation path, derived from a statistical analysis of the scintillation pattern at the two receiving hydrophones, compared favorably with independently determined flow-speed measurements using an Aanderaa current meter, thus demonstrating the viability of the scintillation technique for remote probing of ocean flows. Subsequently, this technique was used to measure flows across a 0.66-km path in a channel, and the results compared well with current measurements obtained from a moored current meter (Farmer and Clifford, 1986). Investigations by Farmer et al. (1987) showed that acoustic scintillation technique can also be used to study the fine structure of turbulent flows. Menemenlis and Farmer (1992) used the scintillation technique to study the ice-water boundary layer. Thus, the path-integral scheme for measurement of turbulence and mixing appears to prove a useful adjunct to the conventional flow measurement techniques. Further investigations have shown that, by spatial filtering of acoustic scintillations from an array of hydrophones, it is possible to obtain horizontal profiles of fine-scale variability and transverse current along short (up to ~2 km) acoustic propagation paths (Farmer and Crawford, 1991; Clay and Medwin, 1977). So far, the application of the acoustic scintillation method is restricted to ranges of less than 1 km because the range is suppressed by ambient noise (Send et al., 2002).

## REFERENCES

- Aki, K., Richards, P.G., 1980. Quantitative Seismology. vol. 2. Freeman, pp. 932.
- Arthur, R.S., Munk, W.H., Issacs, J.D., 1952. The direct construction of wave rays. *Trans. Am. Geophys. Un.* 33, 855–865.
- Behringer, D., Birdsall, T., Brown, M., Cornuelle, B., Heinmiller, R., Knox, R., Metzger, K., Munk, W., Spiesberger, J., Spindel, R., Webb, D., Worcester, P., Wunsch, C., 1982. A demonstration of ocean acoustic tomography. *Nature* 299, 121–125.
- Bowden, K.F., 1954. The direct measurement of subsurface currents in the oceans. *Deep-Sea Res.* 2, 33–47.
- Bretherton, F.P., Davis, R.E., Fandry, C., 1976. A technique for objective analysis and design of oceanographic experiments applied to MODE-73. *Deep-Sea Res.* 23, 559–582.
- Carter, E.F., Robinson, A.R., 1987. Analysis models for the estimation of oceanic fields. *J. Atmos. Ocean. Technol.* 4, 49–74.
- Catherine, A.R., DeRose, J.B., 2004. Investigation of hydroacoustic flow-monitoring alternatives at the Sacramento river at Freeport, California: Results of the 2002–2004 pilot study. Scientific Investigation Report, USGS(2004-5172). Virginia, VA, USA.
- Chen, C.T., Millero, F.J., 1977. Speed of sound in sea water at higher pressure. *J. Acoust. Soc. Amer.* 60, 129–135.
- Chiu, C.L., Hsu, S.M., 2006. Probabilistic approach to modeling of velocity distributions in fluid flows. *J. Hydrology* 316, 28–42.
- Clay, C.S., Medwin, H., 1977. Acoustical oceanography: Principles and applications. Wiley, New York, NY, USA.
- Clifford, S.F., Farmer, D.M., 1983. Ocean flow measurements using acoustic scintillation. *J. Acoustic Soc. Am.* 74, 1826–1832.
- Clifford, S.F., Farmer, D.M., Lataitis, R.J., Crawford, G.B., 1990. Ocean remote sensing by acoustic scintillation techniques. In: Singal, S.P. (Ed.), *Acoustic remote sensing*. Tata McGraw-Hill, Uttar Pradesh, India, pp. 189–197.
- Conzemius, R.J., Montgomery, M.T., 2009. Clarification on the generation of absolute and potential vorticity in mesoscale convective vortices. *Atmos. Chem. Phys. Discuss.* 9, 7531–7554.
- Cornuelle, B., 1983. Inverse methods and results from the 1981 ocean acoustic tomography experiment. Ph.D. Thesis. Massachusetts Institute of Technology/Woods Hole Oceanographic Institution, Cambridge, MA, USA.
- Cornuelle, B.C., Wunsch, C., Behringer, D., Birdsall, T., Brown, M., Heinmiller, R., Knox, R., Metzger, K., Munk, W.H., Spiesberger, J., Spindel, R., Webb, D., Worcester, P., 1985. Tomographic maps of the ocean mesoscale: Pure acoustic. *J. Phys. Oceanogr.* 22, 133–152.
- De Ferrari, H.A., Nguyen, H.B., 1986. Acoustic reciprocal transmission experiments, Florida straits. *J. Acoust. Soc. Amer.* 79, 299–315.
- Duda, T.F., Flatte, S.M., 1988. Modeling meter-scale acoustic intensity fluctuations from oceanic fine structure and microstructure. *J. Geophys. Res.* 93, 5130–5142.
- Dushaw, B.D., Colosi, J.A., 1998. Ray tracing for ocean acoustic tomography, Technical Memorandum. Applied Physics Laboratory, University of Washington, Seattle, WA, USA. TM 3–98.
- Dushaw, B.D., Colosi, J.A., 1998. Ray tracing for ocean acoustic tomography, Applied Physics Laboratory Report. University of Washington, Seattle, WA, USA.
- Elisseeff, P., Schmidt, H., Johnson, M., Herold, D., Chapman, N.R., McDonald, M.M., 1999. Acoustic tomography of a coastal front in Haro Strait, British Columbia. *J. Acoust. Soc. Amer.* 106, 169–184.
- Evensen, G., 1994. Sequential data assimilation with a nonlinear quasi-geostrophic model using Monte Carlo methods to forecast error statistics. *J. Geophys. Res.* 99, 10,143–10,162.
- Farmer, D.M., Crawford, G.B., 1991. Remote sensing of ocean flows by spatial filtering of acoustic scintillations: Observations. *J. Acoustic Soc. Am.* 90, 1582–1591.
- Farmer, D.M., Clifford, S.F., 1986. Space-time acoustic scintillation analysis: a new technique for probing ocean flows. *IEEE J. Oceanic Eng.* OE-11, 42–50.
- Farmer, D.M., Clifford, S.F., Verrall, J.A., 1987. Scintillation structure of a turbulent tidal flow. *J. Geophys. Res.* 92, 5369–5382.
- Gac, C., Gall, Y.L., Terre, T., 1999. For ocean acoustic tomography new modular instrumentation. *Sea Technol.* 40 (3), 55–60.
- Grund, M., Johnson, M., Herold, D., 1997. Haro Strait tidal front mapping experiment. Technical report, Woods Hole Oceanographic Institution. February 1997.
- Gytre, T., 1976. The use of a high-sensitivity ultrasonic current meter in an oceanographic data acquisition system. *Radio and Electronic Engineer* 46 (12), 617–623.
- He, J.M., 2008. The methods to determine stage-discharge relation and examine error. *J. Water Conservancy Science, Technology and Economy* 14 (9), 700–701.

- Herman, G.T., 1980. Image reconstruction from projections: The fundamentals of computerized tomography. Academic Press, Waltham, Massachusetts, USA, pp. 316.
- Herman, G.T. (Ed.), 1979. Image reconstruction from projections: Implementation and applications. Springer-Verlag, London, UK, pp. 284.
- Jensen, F.B., Kuperman, W.A., Porter, M.B., Schmidt, H., 1994. Computational ocean acoustics. American Institute of Physics, New York, NY, USA.
- Kaimal, J.C., 1980. Sonic anemometers. In: Dobson, F., Hasse, L., Davis, R. (Eds.), Air-sea interaction: Instruments and methods. Plenum Press, New York, NY, USA, pp. 81–96.
- Kawanisi, K., Watanabe, S., Kaneko, A., Abe, T., 2009. River acoustic tomography for continuous measurement of water discharge. 3rd International Conference and Exhibition on Underwater Acoustic Measurements: Technologies & Results, 613–620.
- Ko, D.S., De Ferrari, H.A., Malanotte-Rizzoli, P., 1989. Acoustic tomography in the Florida Strait: Temperature, current, and vorticity measurements. *J. Geophys. Res.* 94, 6197–6211.
- Kumar, S.P., Navelkar, G.S., Murthy, T.V.R., Murthy, C.S., 1977. Acoustical characteristics and simulated tomographic inversion of a cold core eddy in the Bay of Bengal. *Acustica-Acta Acustica* 83, 847–854.
- Kumar, S.P., Murty, T.V.R., Somayajulu, Y.K., Chodankar, P.V., Murty, C.S., 1994. Reference sound speed profile and related ray acoustics of Bay of Bengal for tomographic studies. *Acustica* 80, 127–137.
- Larsen, J.C., Sanford, T.B., 1985. Florida current volume transports from voltage measurements. *Science* 227, 302–304.
- Leaman, K.D., Vertes, P.S., Atkinson, L.P., Lee, T.N., Hamilton, P., Waddel, E., 1995. Transports, potential vorticity and current/temperature structure across Northwest Providence and Santaren Channels and the Florida Current off Cay Sal Bank. *J. Geophysical Res. Lett.* 27 (18), 2949–2953.
- Lee, T.N., Schott, F.A., Zantopp, R., 1985. Florida Current: low-frequency variability as observed with moored current meters during April 1982 to June 1983. *Science* 227, 298–302.
- Liebelt, P.B., 1967. An Introduction to Optimal Estimation. Addison-Wesley, Boston, USA.
- Lin, H.Y., 2003. Application of ADCP for river hydrometry. *J. China Water Resources* 9 (B), 37–39.
- Lin, J., Kaneko, A., Gohda, N., Yamaguchi, K., 2005. Accurate imaging and prediction of Kanmon Strait tidal current structures by the coastal acoustic tomography data. *Geophys. Res. Lett.* 32, L14607.
- Lynch, J.F., 1995. Tomography via motion-decoupled surface buoy. *Sea Technol* 36 (9), 25–31.
- Mackenzie, K.V., 1981. Nine-term equation for sound speed in the oceans. *J. Acoust. Soc. Am.* 70, 807–812.
- Madsen, H., Canizares, R., 1999. Comparison of extended and ensemble Kalman filters for data assimilation in coastal area modeling. *Int. J. Numer. Math. Fluids* 31, 961–981.
- Maul, G.A., Chew, F., Bushnell, M., Mayer, D.A., 1985. Sea-level variation as an indicator of Florida Current volume transport: comparisons with direct measurements. *Science* 227, 304–307.
- Medwin, H., 1975. Speed of sound in water: A simple equation for realistic parameters. *J. Acoust. Soc. Am.* 58, 1,318.
- Menemenlis, D., Farmer, D.M., 1992. Acoustic measurement of current and vorticity beneath ice. *J. Atmos. Oceanic Technol.* 9, 827–849.
- Muller, P., Holloway, G., Henyey, F., Pompfrey, N., 1986. Non-linear interactions among internal gravity waves. *Review of Geophysics* 24, 493–536.
- Muller, P., Ren-Chich, L., Williams, R., 1988. Estimates of potential vorticity at small scales in the ocean. *J. Phys. Oceanogr.* 18, 401–416.
- Munk, J.W., Wunsch, C., 1979. Ocean acoustic tomography: A scheme for large scale monitoring. *Deep-Sea Res.* 26A, 123–161.
- Munk, W., Wunsch, C., 1982a. Observing the ocean in the 1990s. *Phil. Trans. Roy. Soc. London A307*, 439–464.
- Munk, W., Wunsch, C., 1982b. Up-down resolution in ocean acoustic tomography. *Deep-Sea Res.* 29, 1415–1436.
- Munk, W., Wunsch, C., 1983. Ocean acoustic tomography: Rays and modes. *Rev. Geophys. and Space Phys.* 21 (4), 777–793.
- Munk, W., Worcester, P.F., Wunsch, C., 1995. Ocean acoustic tomography. Cambridge University Press, New York, NY, USA.
- Nowak, R.T., Mealy, S.F., 1981. Mooring motion monitoring acoustic navigation system. *Proc. IEEE Oceans '81 Conf.*, 793–796.
- Okujima, M., Ohtsuki, S., 1981. Observation of underwater ultrasound propagation in the sea by two-period M-sequence signal method. *Japanese J. Appl. Phys.* 20, 237–239.
- Park, J.H., Kaneko, A., 2000. Assimilation of coastal acoustic tomography data into a barotropic ocean model. *Geophys. Res. Lett.* 27 (20), 3373–3376.
- Parker, R., 1977. Understanding inverse theory. *Ann. Rev. Earth Planet. Sci.* 5, 35–64.
- Pierce, A., 1989. Acoustics: An introduction to its physical principles and application. Acoustical Society of America, New York, NY, USA.
- Rossby, T., 1975. An oceanic vorticity meter. *J. Marine Res.* 33 (2), 213–222.
- Send, U., Worcester, P.F., Cornuelle, B.D., Tiemann, C.O., Baschek, B., 2002. Integral measurements of mass transport and heat content in the Strait of Gibraltar from acoustic transmissions. *Deep-Sea Research II* 49, 4069–4095.
- Simon, M.K., Omura, J.K., Scholtz, R.A., Levin, B.K., 1994. Spread-spectrum communications handbook. McGraw-Hill, New York, NY, USA.
- Spiesberger, J.L., Spindel, R.C., Metzger, K., 1980. Stability and identification of long range ocean acoustic multi-paths. *J. Acoust. Soc. Amer.* 67, 2011–2017.
- Spindel, R.C., 1979. An underwater acoustic pulse compression system. *IEEE Trans. Acoust. Speech and Sig. Proc. ASSP-27*, 723–728.
- Spindel, R.C., Worcester, P.F., 1991. Ocean acoustic tomography: A decade of development. *Sea Technol.* 32 (7), 47–52.
- Spindel, R.C., Worcester, P.F., Webb, D.C., Boutin, P.R., Peal, K.R., Bradley, A.M., 1982. *Proc. IEEE Oceans '82 Conference Record*, 92–99.
- Spindel, R.C., Porter, R.P., Webb, D.C., 1977. A mobile coherent low-frequency acoustic range. *IEEE J. Oceanic Eng.* OE-2, 331–337.
- Spofford, C.W., Stokes, A.P., 1984. An iterative perturbation approach for ocean acoustic tomography. *J. Acoust. Soc. Amer.* 75, 1443–1450.
- Stallworth, L.A., 1973. A new method for measuring ocean and tidal currents. *IEEE Oceans '73*, 55–58.
- Stommel, H., 1955. Direct measurements of subsurface currents. *Deep-Sea Res.* 2, 284–285.
- Suesser, U., 1990. Acoustic propagation in the Strait of Gibraltar, M.Sc. thesis. Royal Roads Military College. British Columbia, Canada, Victoria.

- Takasugi, T., Fujiwara, T., Sugimoto, T., 1994. Formation of sand banks due to tidal vortices around straits. *J. Oceanogr.* 50, 81–98.
- Urick, R.J., 1983. *Principles of Underwater Sound*, third ed. McGraw-Hill, New York, NY, USA.
- Wang, F., Huang, H., 2005. Horizontal acoustic Doppler current profiler (H-ADCP) for real-time open channel flow measurement: Flow calculation model and field validation. In: XXXI IAHR CONGRESS. Seoul, Korea, pp. 319–328.
- Wenz, G.M., 1962. Acoustic ambient noise in the ocean: spectra and sources. *J. Acoust. Soc. Am.* 34, 1936–1956.
- Worcester, P.F., 1977. Reciprocal acoustic transmission in a mid-ocean environment. *J. Acoustic Society of America* 62, 895–905.
- Worcester, P.F., Spindel, R.C., Howe, B.M., 1985. Reciprocal acoustic transmissions: Instrumentation for mesoscale monitoring of ocean currents. *IEEE J. Oceanic Eng.* OE-10, 123–137.
- Wunsch, C., Minster, J.-F., 1982. Methods for box models and ocean circulation tracers: Mathematical programming and nonlinear inverse theory. *J. Geophys. Res.* 87, 5647–5662.
- Yamaguchi, K., Lin, J., Kaneko, A., Yamamoto, T., Gohda, N., H-Nguyen, Q., Zheng, H., 2005. A continuous mapping of tidal current structures in the Kanmon Strait. *J. Oceanography* 61, 283–294.
- Yamaoka, H., Kaneko, A., Park, Jae-Hun, Zheng, H., Gohda, N., Takano, T., Zhu, X.-H., Takasugi, Y., 2002. Coastal acoustic tomography system and its field application. *IEEE J. Oceanic Eng.* 27 (2), 283–295.
- Zhang, C., Zhu, X.-H., Kaneko, A., Wu, Q., Fan, X., Li, B., Liao, G., Zhang, T., 2010. Reciprocal sound transmission experiments for current measurement in a tidal river, 2010 IEEE, Solaris, Singapore.
- Zheng, H., Gohda, N., Noguchi, H., Ito, T., Yamaoka, H., Tamura, T., Takasugi, Y., Kaneko, A., 1997. Reciprocal sound transmission experiment for current measurement in the Seto Inland Sea, Japan. *J. Oceanogr.* 53, 117–127.
- Zhu, X.H., Kaneko, A., Wu, Q., Gohda, N., Zhang, C., Taniguchi, N., 2010. The first Chinese coastal acoustic tomography experiment. Proc. IEEE, Solaris, Singapore.
- Zlotnicki, V., 1983. The oceanographic and geoidal components of sea surface topography. Ph.D. Thesis, MIT/WHOI, Cambridge, MA, USA.
- Chui, C.K., Chen, G., 1991. *Kalman filtering with real-time applications*. Springer, New York, NY, USA.
- Clifford, S.F., Farmer, D.M., 1983. Ocean flow measurements using acoustic scintillation. *J. Acoustic Society of America* 74, 1826–1832.
- Cornuelle, B.D., Worcester, P.F., 1996. Ocean acoustic tomography: Integral data and ocean models. In: Malanotte-Rizzoli, P. (Ed.), *Modern approaches to data assimilation in ocean modeling*. Elsevier, Amsterdam, the Netherlands, pp. 97–115.
- Cornuelle, B., Munk, W., Worcester, P., 1989. Ocean acoustic tomography from ships. *J. Geophys. Res.* 94, 6232–6250.
- Crawford, G.B., Lataitis, R.J., Clifford, S.F., 1990. Remote sensing of ocean flow by spatial filtering of acoustic scintillations: theory. *J. Acoustic Society of America* 88, 442–454.
- Davis, R.E., 1985. Objective mapping by least squares fitting. *J. Geophysical Res.* 90, 4773–4777.
- DeFerrari, H.A., Nguyen, H.B., 1986. Acoustic reciprocal transmission experiments, Florida Straits. *J. Acoustic Society of America* 79, 299–315.
- Deutsch, R., 1965. *Estimation theory*. Prentice-Hall, 269 pp.
- Di Iorio, D., Farmer, D.M., 1996. Two-dimensional angle of arrival fluctuations. *J. Acoustic Society of America* 100, Melville, NY, USA, 814–824.
- Dushaw, B.D., Worcester, P.E., Cornuelle, B.D., Howe, B.M., 1994. Barotropic currents and vorticity in the central North Pacific Ocean during summer 1987 determined from long-range reciprocal acoustic transmissions. *J. Geophys. Res.* 99, 3263–3272.
- Elisseeff, P., Schmidt, H., Johnson, M., Herod, D., Chapman, N.R., McDonald, M.M., 1999. Acoustic tomography of a coastal front in Haro Strait, British Columbia. *J. Acoust. Soc. Am.* 106, 169–184.
- Evensen, G., 2003. The ensemble Kalman filter: Theoretical formulation and practical implementation. *Ocean Dyn.* 53, 343–367.
- Ewart, T.E., Reynolds, S.A., 1978. The mid-ocean acoustic transmission experiment-MATE. *J. Acoust. Soc. Amer.* 63, 1861–1865.
- Farmer, D.M., Di Iorio, D., 1991. Two-dimensional acoustical propagation in a stratified shear flow. In: Potter, J., Warn-Varnas, A. (Eds.), *Ocean variability and acoustic propagation*, Proceedings of the Workshop on Ocean Variability and Acoustic Propagation. Kluwer Academic Publishers, Dordrecht, the Netherlands, pp. 41–55. La Spezia, Italy, June 4–8, 1990.
- Farmer, D.M., Crawford, G.B., 1991. Remote sensing of ocean flows by spatial filtering of acoustic scintillations: observations. *J. Acoustic Society of America* 90, 1582–1591.
- Farmer, D.M., Clifford, S.F., 1986. Space-time acoustic scintillation analysis: a new technique for probing ocean flows. *IEEE Journal of Oceanic Engineering* OE-11, 42–50.
- Flatté, S., Dashen, R., Munk, W.H., Watson, K.M., Zachariasen, F. (Eds.), 1979. *Sound transmission through a fluctuating ocean*. Cambridge University Press, Cambridge, UK.
- Flatté, S.M., Stoughton, R.B., 1986. Theory of acoustic measurement of internal wave strength as a function of depth, horizontal position, and time. *J. Geophysical Res.* 91, 7709–7720.
- Flatté, S.M., Stoughton, R.B., Howe, B.M., 1986. Acoustic measurements of internal wave rms displacement and rms horizontal current off Bermuda in late 1983. *J. Geophysical Res.* 91, 7721–7732.
- Foreman, M.G.G., Walters, R.A., Henry, R.F., Keller, C.P., Dolling, A.G., 1995. A tidal model for eastern Juan de Fuca Strait and the southern Strait of Georgia. *J. Geophys. Res.* 100 (C1), 721–740.

## BIBLIOGRAPHY

- Bellingham, J.G., Schmidt, H., Deffenbaugh, M., 1996. Acoustically focused oceanographic sampling in the Haro Strait experiment. *J. Acoust. Soc. Am.* 100, 2612.
- Canizares, R., Madsen, H., Jensen, H.R., Vested, H.J., 2001. Developments in operational shelf sea modeling in Danish waters. *Estuarine Coastal Shelf Sci.* 53, 595–605.
- Chester, D.B., Malanotte-Rizzoli, P., DeFerrari, H.A., 1991. Acoustic tomography in the Straits of Florida. *J. Geophys. Res.* 96, 7023–7048.
- Chester, D.B., Malanotte-Rizzoli, P., Lynch, J., Wunsch, C., 1994. The eddy radiation of the Gulf Stream as measured by ocean acoustic tomography. *Geophys. Res. Lett.* 21, 181–184.
- Chiu, C.S., Lynch, J.F., Johannessen, O.M., 1987. Tomographic resolution of mesoscale eddies in the Marginal Ice Zone: A preliminary study. *J. Geophys. Res.* 92 (C7), 6886–6902.
- Chiu, C.S., Miller, J.H., Lynch, J.F., 1994. Inverse technique for coastal acoustic tomography. In: Lee, D., Schultz, M.H. (Eds.), *Theoretical and computational acoustics*, 2. World Scientific, Singapore, pp. 917–931.

- Gelb, A. (Ed.), 1974. Applied optimal estimation. MIT Press, Cambridge, MA, USA.
- Hansen, P.C., O'Leary, D.P., 1993. The use of the L-curve in the regularization of discrete ill-posed problems. *SIAM J. Sci. Comput.* 14, 1487–1503.
- Headrick, R.H., Spiesberger, J.L., Bushong, P.J., 1993. Tidal signals in basin-scale acoustic transmissions. *J. Acoust. Soc. Am.* 93, 790–802.
- Howe, B.M., 1987. Multiple receivers in single vertical slice ocean acoustic tomography experiments. *J. Geophys. Res.* 92 (C9), 9479–9486.
- Howe, B.M., Worcester, P.F., Spindel, R.C., 1987. Ocean acoustic tomography: Mesoscale velocity. *J. Geophys. Res.* 92, 3785–3865.
- Hukuda, H., Yoon, J.-H., Yamagata, T., 1994. A tidal simulation of Ariake Bay; A tideland model. *J. Oceanogr.* 50, 141–163.
- Johnson, L.E., Gilbert, F., 1972. Inversion and inference for tele-seismic ray data. *Methods Comp. Phys.* 12, 231–266.
- Kaneko, A., Yamaguichi, K., Yamamoto, T., Godha, N., Zheng, H., Fadli, S., Lin, J., Nguyen, H.Q., 2005. Coastal acoustic tomography experiment in the Tokyo Bay. *Acta Oceanologica Sinica* 24, 86–94.
- Kapoor, T.K., 1995. Three-dimensional acoustic scattering from arctic ice protuberances. Ph.D. thesis. Massachusetts Institute of Technology, Cambridge, MA, USA. June 1995.
- Ko, D.S., DeFerrari, H.A., Malanotte-Rizzoli, P., 1989. Acoustic tomography in the Florida Strait: temperature, current, and vorticity measurements. *J. Geophysical Res.* 94, 6197–6211.
- Lafuente, J.G., Vargas, J.M., Plaza, F., Candela, J., Baschek, B., 2000. Tide at the eastern section of the Strait of Gibraltar. *J. Geophysical Res.* 105 (C6), 14,197–14,213.
- Lawrence, R.S., Ochs, G.R., Clifford, S.F., 1972. Use of scintillations to measure average wind across a light beam. *Applied Optics* 11, 239–243.
- Le Groupe Tourbillon, 1983. The Tourbillon experiment: A study of a mesoscale eddy in the eastern North Atlantic. *Deep-Sea Res.* 30, 475–511.
- Lee, D., 1994. Three-dimensional effects: interface between the Harvard Open Ocean Model and a three-dimensional acoustic model. In: Robinson, A.R., Lee, D. (Eds.), *Oceanography and acoustics: Prediction and propagation models*. AIP, New York, NY, USA.
- Lozano, C.J., Robinson, A.R., Arango, H.G., Gangopadhyay, A., Sloan, Q., Haley, P.J., Anderson, L., Leslie, W., 1996. An interdisciplinary ocean prediction system: assimilation strategies and structured data models. In: Malanotte-Rizzoli, P. (Ed.), *Modern approaches to data assimilation in ocean modeling*. Elsevier, Amsterdam, the Netherlands, pp. 413–452.
- Malanotte-Rizzoli, P. (Ed.), 1996. *Modern approaches to data assimilation in ocean modeling*. Elsevier, Amsterdam, the Netherlands.
- MODE Group, 1978. Mid-ocean dynamics experiments. *Deep-Sea Res.* 25, 859–910.
- Munk, W., Wunsch, C., 1979. Ocean acoustic tomography: A scheme for large-scale monitoring. *Deep-Sea Res.* 26A, 123–161.
- Munk, W., Worcester, P., Wunsch, C., 1995. Ocean acoustic tomography. Cambridge University Press, New York, NY, USA.
- Ocean Acoustic Tomography Group, 1982. A demonstration of ocean acoustic tomography. *Nature* 299, 121–125.
- Paduan, J.D., Gruber, H.C., 1997. Introduction to high-frequency radar: Reality and myth. *Oceanography* 10, 36–39.
- Pan, C.H., Lin, B.Y., Mao, X.Z., 2007. Case study: Numerical modeling of the tidal bore on the Qiantang River, China. *J. J. Hydraulic Eng.* 130–138.
- Park, J.H., Kaneko, A., 2001. Computer simulation of the coastal acoustic tomography by a two-dimensional vortex model. *J. Oceanogr.* 57, 593–602.
- Park, J.-H., Kaneko, A., 2000. Assimilation of coastal acoustic tomography data into a barotropic ocean model. *Geophys. Res. Lett.* 27, 3373–3376.
- Richman, J.G., Wunsch, C., Hogg, N.G., 1977. Space and time scales of mesoscale motion in the western North Atlantic. *Revs. Geophys. Space Phys.* 15, 385–420.
- Robinson, A.R., Carman, J.C., Glenn, S.M., 1994. A dynamical system for acoustic applications. In: Robinson, A.R., Lee, D. (Eds.), *Oceanography and acoustics: Prediction and propagation models*. AIP, New York, NY, USA, pp. 80–117.
- Siegmund, W.L., Lee, D., Botseas, G., Robinson, A.R., Glenn, S.M., 1994. Sensitivity issues for interfacing mesoscale ocean prediction and parabolic acoustic propagation models. In: Robinson, A.R., Lee, D. (Eds.), *Oceanography and acoustics: Prediction and propagation models*. AIP, New York, NY, USA, pp. 133–160.
- Sloat, J.V., Gain, W.S., 1995. Application of acoustic velocity meters for gaging discharge of three low-velocity tidal streams in the St. John River Basin, Northeast Florida. U.S. Geological Survey, Water-Resources Investigations Report, 95–4230.
- Sørensen, J.V.T., Madsen, H., 2004. Efficient Kalman filter techniques for the assimilation of tide gauge data in three-dimensional modeling of the North Sea and Baltic Sea system. *J. Geophys. Res.* 109, C03017.
- Spindel, R.C., Spiesberger, J.L., 1981. Multipath variability due to the Gulf Stream. *J. Acoust. Soc. Amer.* 69, 982–988.
- Takasugi, Y., Fujiwara, T., Sugimoto, T., 1994. Formation of sand banks due to tidal vortices around straits. *J. Oceanogr.* 50, 81–98.
- Takeuchi, T., Taira, K., 1993. Development of multipaths inverted echosounder. In: Teramoto, T. (Ed.), *Deep ocean circulation: Physical and chemical aspects*. Elsevier, Amsterdam, the Netherlands, pp. 375–382.
- Tarantola, A., 1987. *Inverse problem theory: Methods for data fitting and model parameter estimation*. Elsevier, Amsterdam, the Netherlands.
- The ocean tomography group, 1982. A demonstration of ocean acoustic tomography. *Nature* 299, 121375–382125.
- Tiemann, C.O., Worcester, P.F., Cornuelle, B.D., 2001a. Acoustic scattering by internal solitary waves in the Strait of Gibraltar. *J. Acoustic Society of America* 109, 143–154.
- Tiemann, C.O., Worcester, P.F., Cornuelle, B.D., 2001b. Acoustic remote sensing of internal solitary waves and internal tides in the Strait of Gibraltar. *J. Acoustic Society of America* 110 (2), 798–811.
- Wolanski, E., Williams, D., Spagnol, S., Chanson, H., 2004. Undular tidal bore dynamics in the Daly Estuary, Northern Australia. *J. Estuarine, Coastal and Shelf Science* 60, 629–636.
- Worcester, P., 1981. An example of ocean acoustic multi-path identification at long range using both travel time and vertical arrival angle. *J. Acoust. Soc. Amer.* 70, 1743–1747.
- Worcester, P.F., 1977. Reciprocal acoustic transmission in a mid-ocean environment. *J. Acoust. Soc. Amer.* 62, 895–905.
- Worcester, P.F., 1979. Reciprocal acoustic transmission in a mid-ocean environment: fluctuations. *J. Acoust. Soc. Amer.* 66, 1173–1181.
- Worcester, P.F., Dushaw, B.D., Howe, B.M., 1991. Gyre-scale reciprocal acoustic transmissions, pp. 119–134. In: Potter, J., Warn-Varnas, A. (Eds.), *Ocean variability and acoustic propagation*. Kluwer, Dordrecht, the Netherlands.

- Worcester, P.F., Williams, G.O., Flatté, S.M., 1981. Fluctuations of resolved acoustic multipaths at short range in the ocean. *J. Acoust. Soc. Amer.* 70, 825–840.
- Worcester, P.F., Send, U., Cornuelle, B.D., Tiemann, C.O., 1997. Acoustic monitoring of flow through the Strait of Gibraltar. In: Zhang, R., Zhou, J. (Eds.), *Shallow-Water Acoustics, Proceedings of the International Conference on Shallow Water Acoustics*. China Ocean Press, Beijing, China, pp. 471–477. April 21–25, 1997.
- Yamaoka, H., Kaneko, A., Park, J.-H., Zheng, H., Gohda, N., Takano, T., X-Zhu, H., Takasugi, Y., 2002. Coastal acoustic tomography system and its field application. *IEEE J. Oceanic Eng.* 27 (2), 283–295.
- Yanagi, T., 1989. *Coastal oceanography*. Koseisha-Koseikaku, Tokyo, Japan (in Japanese).
- Zheng, H., 1997. Study on development and application of the coastal acoustic tomography system, Ph.D. dissertation. Hiroshima University, Japan.
- Zheng, H., Yamaoka, H., Gohda, N., Noguchi, H., Kaneko, A., 1998. Design of the acoustic tomography system for velocity measurement with an application to the coastal sea. *J. Acoust. Soc. Jpn. (E)* 19, 199–210.
- Zheng, H., Gohda, N., Noguchi, H., Ito, T., Yamaoka, H., Tamura, T., Takasugi, Y., Kaneko, A., 1997. Reciprocal sound transmission experiment for current measurement in the Seto Inland Sea, Japan. *J. Oceanogr.* 53, 117–127.
- Zhu, X.H., Gohda, N., Wu, Q.S., Naowa, T., Zhang, C.Z., 2009. Acoustic current meter for measurement of velocity in a shallow channel. *J. Electronic Measurement Technology* 32 (2), 166–169.